

Assumed Probability Density Functions for Shallow and Deep Convection

Peter A. Bogenschutz¹, Steven K. Krueger¹ and Marat Khairoutdinov²

¹ Department of Atmospheric Science, University of Utah, Salt Lake City, Utah

² School of Marine and Atmospheric Sciences, Stony Brook University, Stony Brook, New York

Manuscript submitted 26 May 2010; in final form 20 September 2010

The assumed joint probability density function (PDF) between vertical velocity and conserved temperature and total water scalars has been suggested to be a relatively computationally inexpensive and unified subgrid-scale (SGS) parameterization for boundary layer clouds and turbulent moments. This paper analyzes the performance of five families of PDFs using large-eddy simulations of deep convection, shallow convection, and a transition from stratocumulus to trade wind cumulus. Three of the PDF families are based on the double Gaussian form and the remaining two are the single Gaussian and a Double Delta Function (analogous to a mass flux model). The assumed PDF method is tested for grid sizes as small as 0.4 km to as large as 204.8 km. In addition, studies are performed for PDF sensitivity to errors in the input moments and for how well the PDFs diagnose some higher-order moments.

In general, the double Gaussian PDFs more accurately represent SGS cloud structure and turbulence moments in the boundary layer compared to the single Gaussian and Double Delta Function PDFs for the range of grid sizes tested. This is especially true for small SGS cloud fractions. While the most complex PDF, Lewellen-Yoh, better represents shallow convective cloud properties (cloud fraction and liquid water mixing ratio) compared to the less complex Analytic Double Gaussian 1 PDF, there appears to be no advantage in implementing Lewellen-Yoh for deep convection. However, the Analytic Double Gaussian 1 PDF better represents the liquid water flux, is less sensitive to errors in the input moments, and diagnoses higher order moments more accurately. Between the Lewellen-Yoh and Analytic Double Gaussian 1 PDFs, it appears that neither family is distinctly better at representing cloudy layers. However, due to the reduced computational cost and fairly robust results, it appears that the Analytic Double Gaussian 1 PDF could be an ideal family for SGS cloud and turbulence representation in coarse-grid CRMs, mesoscale models, and GCMs if the required input moments can be predicted or diagnosed accurately.

DOI:10.3894/JAMES.2010.2.10

1. Introduction

The need for improved representations of clouds in climate models has been long recognized (Arakawa 2004). The importance of realistic cloud representation rests in the fact that clouds have prominent, yet highly uncertain, feedbacks on the climate system. Recently a method known as the Multi-Scale Modeling Framework (MMF; Grabowski and Smolarkiewicz 1999), in which a cloud resolving model (CRM) is placed within each grid cell of a general circulation model (GCM), has proven to be a promising approach for the better understanding of the role of clouds in climate (Randall et al. 2003; Khairoutdinov et al. 2005). The MMF differs from a traditional cloud parameterization because it resolves most cloud-forming processes, whereas a traditional

parameterization estimates the unresolved cloud processes from the resolved large-scale fields using a simple set of rules.

While the MMF shows great promise towards the goal of improving the representation of clouds in climate models (Randall et al. 2003), the method is computationally expensive. For example, with current computational abilities, the embedded 2D CRM in the Colorado State University's super-parameterized-Community Atmospheric Model (SP-CAM, Khairoutdinov et al. 2005) is limited to a horizontal grid size of 4 km and domain size of 128 to 256 km. This is considered to be a coarse grid for a CRM and is perhaps adequate to resolve deep convective processes and mesoscale convective systems, but certainly not shallow convection.

To whom correspondence should be addressed.

Peter Bogenschutz, Atmospheric Sciences, University of Utah, 135 S 1460 East Rm 819 (WBB), Salt Lake City, UT 84112-0110, USA
P.Bogenschutz@utah.edu



This work is licensed under a Creative Commons Attribution 3.0 License.

Shallow convective cloud systems, such as stratocumulus and trade wind cumulus, significantly affect the global radiation budget and play an important role in the energy and hydrological cycles of the atmosphere (Slingo 1990). On shorter time scales, Khairoutdinov and Randall (2006) showed that cold pools formed by the evaporation of precipitation from shallow convection over land is important for the development and organization of deep convection. Incorporation of the effects of shallow cumulus clouds into numerical models has been a significant challenge since the clouds have characteristic sizes that are much smaller than the grid boxes in many types of numerical models, including GCMs, mesoscale models, and even CRMs. For the time being, it remains computationally unfeasible for a CRM used in MMF to have a grid spacing fine enough to resolve shallow convection with domain sizes of 128 to 256 km. Therefore, improved and unified SGS cloud and turbulence parameterizations are needed in these embedded coarse-grid CRMs, with an important emphasis on keeping them economical.

Historically, boundary layer clouds and turbulence have been parameterized using a variety of methods. Among them are higher-order turbulence closure models (e.g. Bougeault 1981a,b; Krueger 1988; Redelsperger and Sommeria 1986), low-order closure models (e.g. Bechtold et al. 1992; Khairoutdinov et al. 2003), and mass flux models (e.g. Arakawa and Schubert 1974). In general, these methods are either too computationally expensive or not general and therefore require case specific adjustments for particular regimes. However, the three basic closures mentioned have been combined into a single scheme in an attempt to create a unified parameterization. An example is that of Lappen and Randall (2001), in which a variety of cloud regimes were represented with a single parameterization. Their parameterization combined the mass-flux and higher-order closure approaches. The scheme was tested on a dry convective boundary layer, a stratocumulus-topped layer, and a trade wind cumulus layer. The two former cases agreed well with observations. However the trade wind cumulus case produced cloud fractions that were too high.

Golaz et al. (2002a) proposed a scheme more complicated than that of Lappen and Randall (2001). Golaz et al. (2002a) developed a single column model that predicts the triple joint probability density function (PDF) of vertical velocity, liquid water potential temperature (θ_l), and total water mixing ratio (q_t). The mass flux, turbulent moments, and cloud fraction can be easily diagnosed once the PDF ($P(w, \theta_b, q_t)$) is known. However, a functional form of the PDF must be assumed (known as the “assumed PDF method”) since explicitly predicting the PDF is computationally demanding. Therefore, one must choose a PDF family to use. Golaz et al. (2002b) chose a family of double Gaussian PDFs. Their decision was based on a study by Larson et al. (2002) that evaluated the performance of several families of joint PDFs, and found that cloudy

boundary layer PDFs more closely resembled double Gaussians than double delta functions or single Gaussians.

Several advantages of the PDF method are listed in Golaz et al. (2002a). Cloud properties (cloud fraction and liquid water mixing ratio), high order moments, and buoyancy terms can be computed from the same PDF. The PDF parameterization is also flexible, meaning that the family of PDFs used can be changed without rewriting the parameterization completely. Finally, based on the PDF used, the PDF parameterization can be general so a single scheme can be applied to all cloud regimes and is able to simulate transitions from one regime to another. This paper aims to evaluate which PDFs are most likely to provide unified results and for a wide range of horizontal grid box sizes.

This paper presents results from an extensive assessment of PDF families including: Double Delta Function, Single Gaussian, Lewellen-Yoh (Lewellen and Yoh 1993), and Analytic Double Gaussians 1 and 2 for three different cloud regimes and a variety of grid sizes. We aim to select a PDF that can parameterize unresolved turbulence and clouds for 2D and 3D coarse-grid CRMs and that can be incorporated into the MMF with minimal computational expense.

This study is an extension of Larson et al. (2002). Larson et al. (2002) tested the assumed PDFs against aircraft observations and LES results from simulated boundary layer clouds (shallow cumulus and stratocumulus). They concluded that the Lewellen-Yoh PDF had the best fits for cloud fraction, liquid water mixing ratio, and liquid water flux. We evaluate assumed PDFs for deep convection and a transition case from stratocumulus to cumulus. In addition our results include a broader range of grid sizes and more robust statistics. The PDFs are tested for grid box sizes ranging from 0.2 km to 204.8 km, therefore testing the PDFs for grid sizes characteristic for CRMs, mesoscale models, and GCMs. Two other unique aspects of this study are that the PDFs are tested to determine how sensitive they are to errors introduced to the input moments and are evaluated for the higher order moments that are typically needed to close model equations (e.g. w'^4 , $w'^2\theta'_v$, $q'_t\theta'_v$, $\theta'_t\theta'_v$). The main focus of the Larson et al. (2002) study was an evaluation of PDF performance compared to aircraft observations whereas ours focuses on evaluation with LES data.

The format of the paper is as follows: Section 2 discusses SAM, the model used for this research. Section 3 discusses the three high resolution benchmark cases used for this study. Section 4 describes the assumed PDFs used and how they are evaluated with respect to the high resolution benchmark cases. Results are presented in section 5, while section 6 discusses conclusions and plans for future work.

2. Model Description

The System for Atmospheric Modeling (SAM) was developed by Marat Khairoutdinov at Colorado State University (CSU). A thorough description of the model, including formulation of model equations and microphy-

sics, can be found in Khairoutdinov and Randall (2003). The prognostic thermodynamical variables for SAM are the liquid water/ice moist static energy, total nonprecipitating water (vapor + cloud water + cloud ice), and total precipitating water (rain + snow + graupel). Cloud condensate (cloud water + cloud ice) is diagnosed using the “all or nothing” approach, thus a grid box is assumed to be either completely cloudy or completely clear. The sub-grid scale model for SAM includes two options: a 1.5-order closure using a prognostic equation for the sub-grid scale turbulent kinetic energy or a simple Smagorinsky-type closure. Periodic lateral boundary conditions are employed with a rigid lid at model top above a sponge layer. Surface fluxes are computed using Monin-Obukhov similarity.

3. Large-Eddy Benchmark Simulations

Three large-eddy benchmark simulations were performed to collect robust statistical moments for a range of grid sizes that can be used to test the assumed PDF method. The first is a case of trade wind cumulus (Cu) derived from the Barbados Oceanographic and Meteorological Experiment (BOMEX). This is a steady and non-precipitating case and was selected due to the importance of including the trade wind Cu regime in convection schemes and GCMs (Tiedtke 1988). The second case is a transition case from stratocumulus to cumulus (hereafter denoted as TRANS). TRANS provides a range of non-precipitating cloud regimes that includes stratocumulus (Sc), cumulus under Sc, and trade wind Cu. Here we focus our attention on the cumulus-under-stratocumulus intermediate regime (Bretherton 1993; Klein et al. 1995). The third case is an idealized GATE¹ case, which is a high resolution and large domain steady case of precipitating deep convection with mesoscale organization (Khairoutdinov et al. 2009).

3.1. BOMEX

The trade cumulus case selected is one derived from BOMEX which took place on 22–30 June 1969 (Holland and Rasmusson 1973). We ran the case using the setup as outlined by the Global Energy and Water Cycle Experiment (GEWEX) Cloud System Studies (GCSS) boundary layer working group I (complete case summary found at <http://www.knmi.nl/~siebesma/gcss/bomex.html>). The standard case (Siebesma et al. 2003) is run in a 6.4 km × 6.4 km domain. However in order to test a wider range of grid sizes for the PDFs, we chose to run a 25.6 km × 25.6 km domain case with 100-m horizontal resolution.

The horizontal and temporally averaged 100 m LES liquid water mixing ratio (q_l) and cloud fraction profiles for this run can be found in Fig. 1 (black line), for the entire six hour simulation. Here we find cloud base at approximately

¹Global Atmospheric Research Program (GARP) Atlantic Tropical Experiment

500 m, or at the bottom of the conditionally unstable layer, with clouds extending up to near 2 km. The maximum cloud fraction produced by the 100 m benchmark is 6% at cloud base. Many parameterizations have difficulty in simulating the small cloud fraction of this trade-wind cumulus case (Lappen and Randall 2001).

3.2. Transition from Stratocumulus to Cumulus (TRANS)

A simulation of the transition from stratocumulus to trade cumulus (TRANS) was performed with initial soundings based on observations taken on the Ocean Weather Ship N (30°N, 140°W; Klein et al. 1995). We modified the profiles to make them more similar to those used by Krueger et al. (1995), who performed a Lagrangian simulation using a July climatological boundary-layer trajectory over the northeastern Pacific southwest of California. This simulation employs interactive radiation, and SSTs warm linearly from 290 to 305 K throughout the seven-day simulation. The standard simulation has a 3.2 km × 3.2 km domain with a 50 m horizontal grid size. However, in order to test a wider range of grid sizes for the PDFs, we chose to run a 25.6 km × 25.6 km domain case with a 50 m horizontal grid size.

3.3. Giga-LES

A Large-Eddy Simulation (LES) was executed in an attempt to apply LES resolution to simulate deep tropical convection in a domain comparable of a typical horizontal grid cell in a GCM (Khairoutdinov et al. 2009). This simulation (hereafter referred to as the “Giga-LES” due to the computation size) is unique in that the domain is large enough to simulate deep convection and mesoscale organization, yet has a resolution fine enough to resolve the shallow convection and boundary layer turbulence. Moeng et al. (2009) examined the boundary layer properties of this simulation and also evaluated a typical SGS model commonly used in CRMs. Their results suggest that simple downgradient diffusion closure used in CRMs cannot adequately represent fluxes of conserved scalars in the maritime boundary layer under deep convection.

The Giga-LES is an idealized simulation using GATE Phase III mean conditions, with a sheared profile in the zonal wind (Fig. 1 of Khairoutdinov et al. 2009). The domain size is 204.8 km by 204.8 km in the horizontal, with the model top reaching approximately 27 km. The horizontal grid size is 100 m in each direction with the vertical grid spacing ranging from 50 m in the boundary layer to 300 m near model top. Therefore, the Giga-LES utilizes a grid of 2048 × 2048 × 256 (more than a billion) points. Periodic lateral boundary conditions are applied and small random temperature noise is used at the lowest grid levels to initiate turbulence. Large scale advective and radiative tendencies of temperature and water vapor are applied

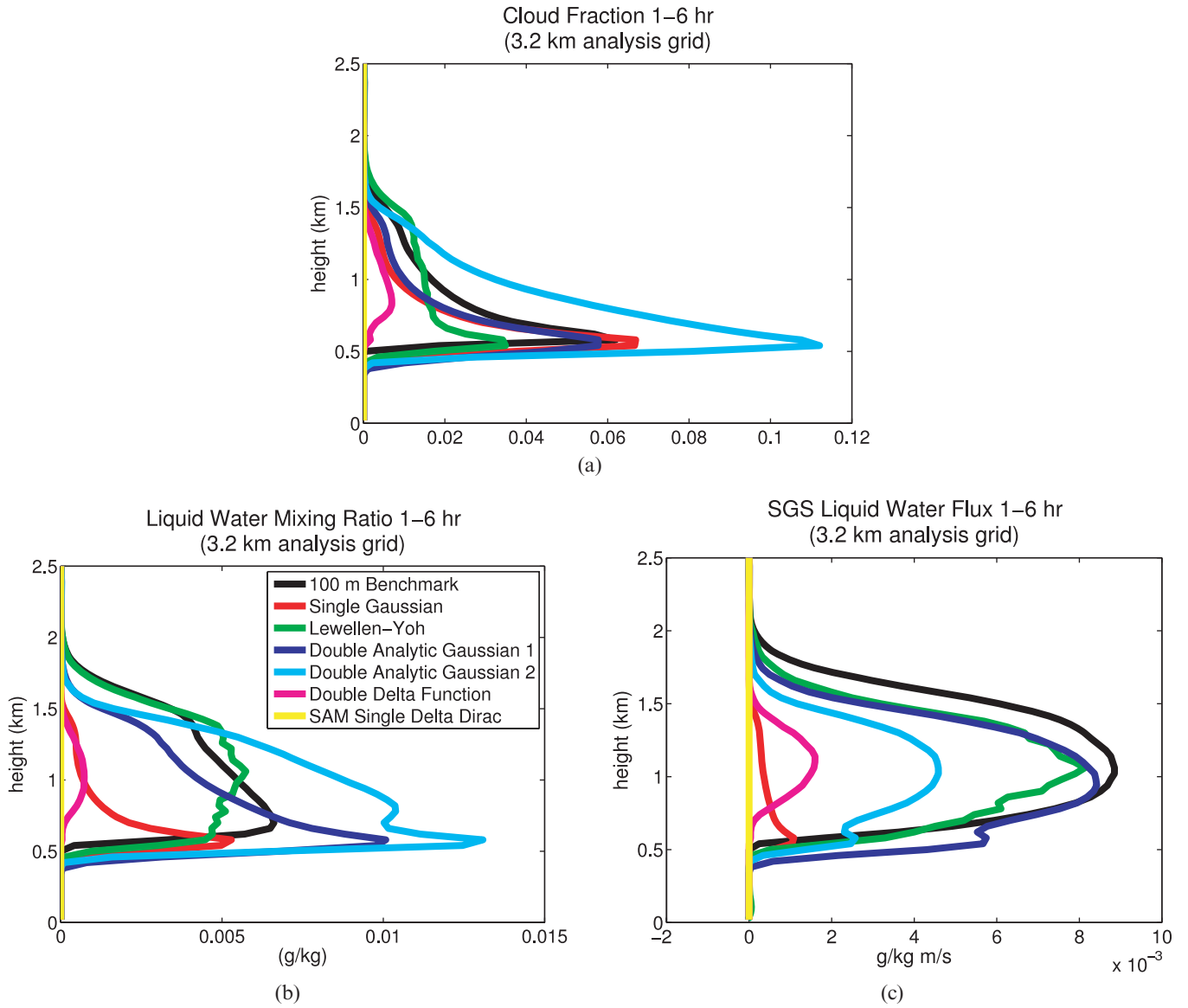


Figure 1. Horizontally and temporally averaged output profiles from the various PDFs of cloud fraction, liquid water mixing ratio, and liquid water flux for the 3.2 km analysis grid (i.e. input moments averaged on a 3.2 km grid) over the six hour simulation for the 25.6 km domain BOMEX case.

continuously. The Giga-LES used a time step of 2 seconds and simulated a 24 hour period.

4. Evaluation of PDFs

4.1. Description of PDFs

Five three-dimensional joint PDFs of $P(w, \theta_b, q_t)$ were analyzed for this study to determine which would be most suitable to use in coarse-grid CRM turbulence parameterizations. These five PDFs are the Double Delta Function (DDF), Single Gaussian (SG), Lewellen-Yoh (LY; Lewellen and Yoh 1993), Analytic Double Gaussian (ADG) 1 and ADG2. In addition, SAM’s existing Single Delta Function

(SDF) or “all or nothing” condensation scheme will also be subject to our evaluation. Table 1 contains a summary of the input moments required for each PDF. Larson et al. (2002)

Table 1. Summary of input moments for each assumed PDF.

Assumed PDF	Required Input Moments
Single Delta Function (SDF)	$\bar{\theta}, \bar{q}_t$
Double Delta Function (DDF)	$\bar{w}, \overline{w^2}, \overline{w^3}, \bar{\theta}_1, \bar{q}_1, \overline{w'q'_t}, \overline{w'\theta'_1}$
Single Gaussian (SG)	$\bar{w}, \overline{w^2}, \bar{\theta}_1, \overline{\theta_1^2}, \bar{q}_1, \overline{q_1^2}, \overline{w'q'_t}, \overline{w'\theta'_1}, \overline{q'_t\theta'_1}$
Lewellen-Yoh (LY)	$\bar{w}, \overline{w^2}, \overline{w^3}, \bar{\theta}_1, \overline{\theta_1^2}, \overline{\theta_1^3}, \bar{q}_1, \overline{q_1^2}, \overline{q_1^3}, \overline{w'q'_t}, \overline{w'\theta'_1}, \overline{q'_t\theta'_1}$
Analytic Double Gaussian 1 (ADG1) and 2 (ADG2)	$\bar{w}, \overline{w^2}, \overline{w^3}, \bar{\theta}_1, \overline{\theta_1^2}, \bar{q}_1, \overline{q_1^2}, \overline{w'q'_t}, \overline{w'\theta'_1}, \overline{q'_t\theta'_1}$

provided complete formulations for each PDF, so only a brief description and review of PDF performance in previous studies will be given here.

In general, a DDF PDF is similar to a mass-flux scheme which only consists of updraft and downdraft plumes and with no subplume variability. While the DDF requires the least number of input moments and is the simplest of the proposed PDFs that permits nonzero skewness, the DDF has been found to be unsatisfactory. Larson et al. (2002) concluded that atmospheric PDFs resemble double Gaussians more than DDFs. The DDF tends to misrepresent the tail of the distribution of shallow cumulus, which leads to an underestimation of cloud properties such as cloud fraction and q_l .

On the other hand, the SG does not permit skewness or bimodality but, unlike the DDF, it does represent the scalar variances of $\theta_l'^2$ and $q_l'^2$. The SG PDF is arguably the least complex family, due to the fact that it does not require w'^3 or any other third order moments, as an input. As already stated, trade wind Cu have cloud and turbulence properties that are highly skewed. While the SG would be an acceptable PDF to apply to a stratocumulus layer, due to the highly Gaussian nature of that regime and low complexity of the PDF, it would likely fail for a regime characterized by low cloud fraction. We desire a PDF which is able to diagnose a variety of cloud type regimes without regime-specific adjustments.

The LY PDF is based on a double Gaussian function. It is the most complex of the PDFs tested in this study and it requires the most input moments. This PDF is determined by the means, variances, and covariances of w , θ_b , and q_b plus w'^3 , $\theta_l'^3$, and $q_l'^3$. In addition, the PDF parameters for the LY family cannot be obtained analytically. They require a numerical root finder and hence LY is a more computationally expensive PDF. However, Larson et al. (2002) found that the LY PDF had the best fits of the PDFs tested.

Both of the ADG PDFs are based on the double Gaussian shape. However, they each have fewer input parameters compared to the LY PDF. Namely, the ADG PDFs do not require $q_l'^3$ or $\theta_l'^3$. In addition, the ADG PDF parameters can be found analytically, as the name suggests. This quality is desirable, should the PDF parameterization be implemented into a MMF. However, both ADG PDFs make fairly rigid assumptions, when compared to LY, in defining the widths of the two plumes for w and the within plume correlations. For instance, ADG1 assumes the widths of each Gaussian PDF for vertical velocity are equal and set constant. This assumption is alleviated somewhat in the ADG2 PDF, where the widths of the individual Gaussians in w are found using the formulas of Luhar et al. (1996). The definition of the widths for w is the only difference between ADG1 & 2. Both of these PDFs assume the within plume correlations of vertical velocity and the thermodynamic scalars are zero. Despite these simplifying assumptions, Larson et al. (2002) found that both of the ADG PDFs provided good results, they tend to fit low-cloudiness cumulus layers better than the single Gaussian PDF.

4.2. Analysis of PDFs

During model integration, various statistical moments were computed for a range of horizontal grid sizes. A total of thirty-one moments were computed, which includes all the second and third order moments needed for input into the PDFs. Also included were important quantities such as cloud fraction, $\overline{q_l}$, and $\overline{w'q_l'}$; as well as terms that higher order closure models need to close their equations, such as $\overline{w'^2 q_l'}$, $\overline{\theta_l' q_l'}$, and $\overline{q_l' q_l'}$. All of the mentioned quantities can be used to test the diagnosed output from each of the assumed PDFs. Simple box averaging is used to compute the input moments for a particular analysis grid size, given as

$$\overline{\phi'^m} = \frac{1}{n} \sum_{i=1}^{i=n} (\phi_i - \overline{\phi})^m, \quad (1)$$

$$\overline{\phi} = \frac{1}{n} \sum_{i=1}^{i=n} \phi_i, \quad (2)$$

where ϕ_i is any variable from LES, n is the number of LES grid points in the analysis grid box size, and $\overline{\phi}$ is the averaged ϕ over the particular analysis grid box being considered.

The computation of the moments and diagnostics for various grid sizes (ranging from 0.4 km to 204.8 km, depending on the case) allows us to test the assumed PDF method for a variety of horizontal grid sizes. These grid sizes range from typical spacing used in CRMs (0.4 to 3.2 km), mesoscale models (6.4 to 12.8 km), and large scale or GCMs (25.6 km and higher). For the purpose of this study, we are most interested on assessing the performance of the assumed PDF method for a grid size typically used by the embedded CRM in the MMF (3.2 km or even 6.4 km). However, it is useful to assess the performance of the assumed PDFs for larger grid sizes for potential application of the parameterization in mesoscale models or directly in GCMs.

For the first portion of the study, we focus our analysis on variables related to cloud structure: C (cloud fraction), and q_n (nonprecipitable cloud condensate mixing ratio, from which both q_l and q_i can be diagnosed). We also analyze results for the liquid water flux ($\overline{w'q_l'}$), which is a key term in the computation of buoyancy flux (g/θ_o) $\overline{w'\theta_l'}$. We use:

$$\begin{aligned} \overline{w'\theta_l'} &= \overline{w'\theta_l'} + \frac{1-\varepsilon}{\varepsilon} \theta_o \overline{w'q_l'} \\ &+ \left[\frac{L_v}{c_p} \left(\frac{p_o}{p} \right)^{R_d/c_p} - \frac{1}{\varepsilon} \theta_o \right] \overline{w'q_l'} \end{aligned} \quad (3)$$

where $\varepsilon = R_d/R_v$, R_d is the gas constant for dry air, R_v is the gas constant of water vapor, L_v is the latent heat of vaporization, c_p is the heat capacity of air, θ_o is a reference

temperature, p is the pressure, and p_o is a constant reference pressure. The derivation of equation 4.3 can be found in Randall (1980). Since $w'\theta'_l$ and $w'q'_l$ are inputs to the PDFs (i.e., are either diagnosed or predicted by the host model), the choice of the selected PDF family will determine how accurately $w'\theta'_v$ is diagnosed, based solely on how well $w'q'_l$ is diagnosed. Accurate representation of $w'q'_l$ is very important for turbulence parameterizations given that $(g/\theta_o)w'\theta'_v$ is the most important source term for TKE in cloudy layers.

The later portion of the study (for the BOMEX case) focuses on the evaluation of PDFs for diagnosing some higher order moments that are typically needed to close the second and third order moment prognostic equations. These terms include w'^4 , $w'^2\theta'_v$, $q'_l\theta'_v$, and $\theta'_l\theta'_v$.

It is extremely important to note that this analysis of the assumed PDFs is being conducted assuming “perfect moments”. The purpose of this study is to determine which PDF has the most potential of successfully being implemented as a parameterization in the best case scenario. However, we also test to determine the sensitivity of the PDFs to errors introduced into the perfect input moments.

5. Results

5.1. PDF Results from a BOMEX Simulation of Trade Cumulus

Spatially and temporally averaged profiles of cloud fraction, liquid water mixing ratio, and liquid water flux, from the entire six-hour simulation, for the PDFs for the 3.2 km analysis grid size are shown in Fig. 1. The moderately-complex ADG1 does a good job of representing the trade cumulus in this case. While this PDF overestimates q_l at cloud base, the horizontally and temporally averaged profiles of cloud fraction and $w'q'_l$ strongly resemble the averaged profiles of the 100-m benchmark case. SG appears to diagnose the cloud fraction quite well. However it grossly underestimates q_l and $w'q'_l$ above cloud base. DDF misrepresents the cloud base height and also underestimates all quantities.

The most complex PDF, LY, is the only one to accurately diagnose the cloud base and cloud top levels. However, cloud fraction values at cloud base are negatively biased and LY inaccurately diagnoses the height of the maximum q_l . ADG2 does not fare quite as well as ADG1 and LY, with overestimations of C and q_l at nearly every level, especially at cloud base, and an underestimation of $w'q'_l$. The SAM SDF “all or nothing” approach performs the poorest, diagnosing only clear skies. As shown in Fig. 1(c), all PDFs underestimate the liquid water flux to some degree. While not shown, profiles for the 6.4 km grid exhibit little difference compared to 3.2 km analysis grid profiles.

The correlation coefficient, RMSE, and mean bias (computed with respect to grid averaged quantities derived from the 100 m benchmark case) for the various grid sizes are shown in Fig. 2 for q_l . RMSE tells us the typical magnitude of errors (the difference between “forecast” and

“observation” are squared then averaged), while mean bias is an indicator of the the “direction” of the errors (the differences between “forecast” and “observation” are simply averaged). For the double Gaussian based PDFs (LY, ADG1 and ADG2) we see correlation scores that are relatively insensitive to grid spacing, with LY scoring the highest. However, for SG and DDF, there is a significant drop in correlation scores with increasing grid size due to the fact that DDF fails to diagnose any clouds for the coarse grid sizes and SG only diagnoses q_l at cloud base, with extreme under-representation in the mid-cloud layer where clouds tend to be less numerous. The SAM SDF fails to diagnose any clouds for grid sizes larger than 0.4 km. While ADG2 suffers from relatively high error and bias for the intermediate grid sizes, ADG1 and LY perform the best.

Correlation statistics for the liquid water flux (Fig. 3) show even less sensitivity to the grid size for the three double-Gaussian-based PDFs. This is especially true for ADG1, and while ADG1 does exhibit higher error for the fine grid sizes, it also has the lowest error and bias for the important intermediate grid box sizes of 3.2 and 6.4 km. The less complex PDFs exhibit strong negative biases for cloud fraction, q_b and $w'q'_l$. Overall, it appears that both LY and ADG1 are the best performing PDFs for this shallow cumulus regime and the lack of sensitivity to grid size for these PDFs suggest that they may provide the basis for a unified parameterization when applied to a range of grid box sizes.

Examples of projected PDFs from SG and ADG1 in midcloud layer for the 25.6 km grid size are shown in Fig. 5, with the 100 m benchmark PDF in Fig. 4. This example illustrates how the SG typically underestimates the cloud fields for this regime, due to the lack of skewness in the PDF. On the other hand, the ADG1 PDF has tails in all three fields that are representative of the cumulus portion of the PDF. For this particular example, the SG PDF underestimated q_l by a factor of 10, whereas ADG1 compared nicely to the benchmark simulation. An examination of the ADG2 PDF (not shown) highlights the differences between this PDF and ADG1. ADG2 tends to diagnose widths and amplitudes of the cumulus PDF that are too large for trade wind cumulus layers, thus resulting in an overrepresentation of cloud fraction and q_l . The ADG1 assumes that the widths for the w plumes are equal, which apparently is a better approximation than that used in ADG2 for trade cumulus.

5.2. Results from a Transition Simulation of Stratocumulus to Cumulus

The evolution of the horizontally averaged profiles of cloud fraction are shown in Fig. 6. The 50-m grid size LES (Fig. 6(a)) exhibits high cloud fractions for the first day and a half, which is representative of the stratocumulus regime, with an obvious diurnal pattern. After the second day, the regime gradually transitions to that of a trade cumulus and after the fourth day the cloud layer begins to slowly deepen and decouple from the mixed layer.

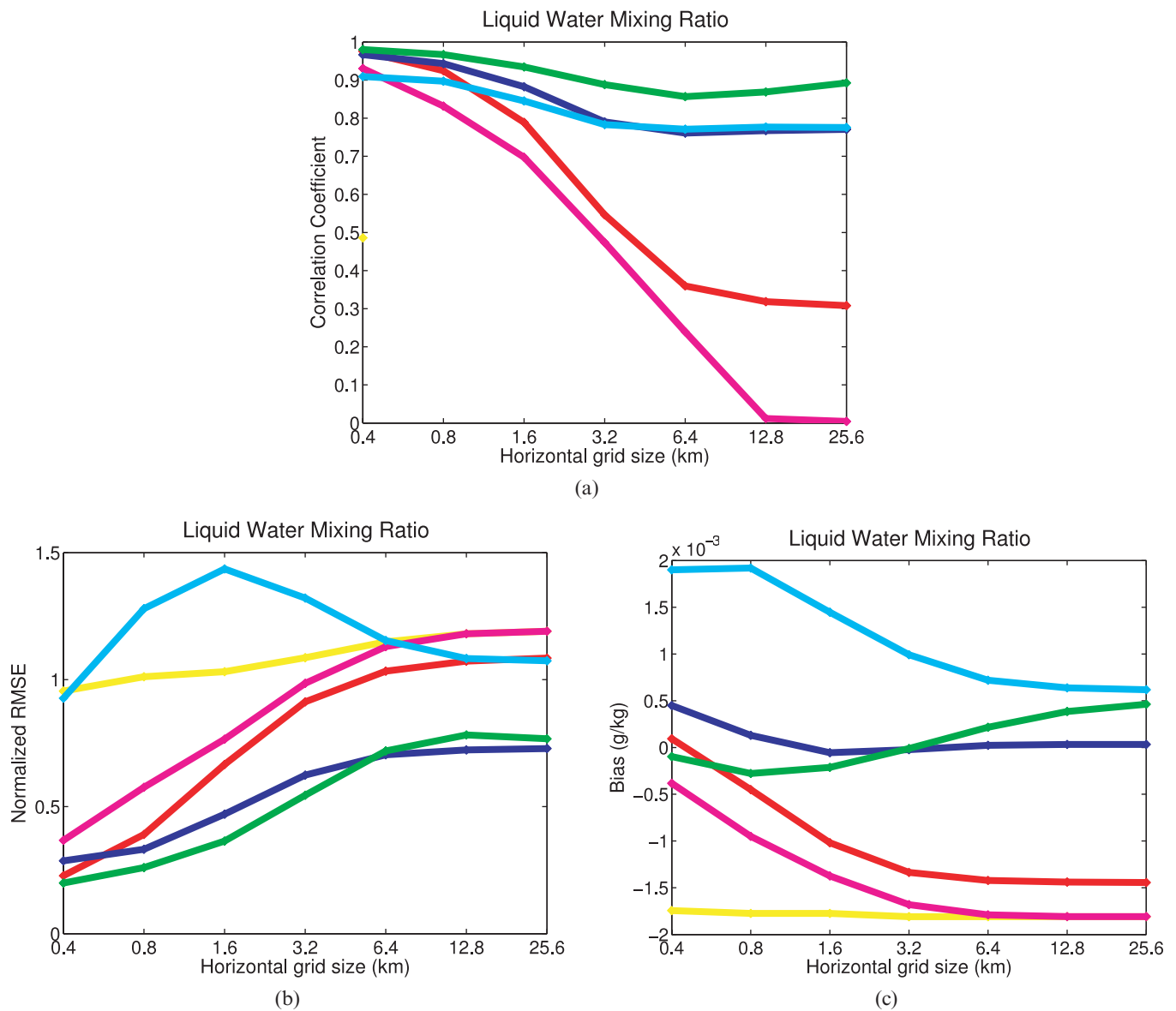


Figure 2. Statistics for liquid water mixing ratio for the BOMEX simulation for hours 3–6 for all levels. Color scheme same as Fig. 1.

Figures 6(b) and 6(c) represent results of ADG1 and SDF utilizing perfect moments from LES results for a 3.2-km analysis grid. All three of the double Gaussian PDFs do an excellent job of representing the structure and evolution of the cloud regimes for the 3.2-km analysis grid (although not shown the LY and ADG2 results are comparable to the ADG1 results). The SG and DDF PDFs (not shown), for the 3.2 km analysis grid size, accurately represent the stratocumulus portion of the simulation but underestimate the cloud fraction for the trade cumulus phase. Even at large grid sizes, all the way to 25.6 km (not shown), the three double Gaussian PDFs still diagnose the cloud structure reasonably well for the entire simulation, while the rest of the PDFs fail to do so.

The rest of the analysis will focus on the third day, when the intermediate boundary-layer regime, characterized by

cumulus-under-stratocumulus cloud type, is present. The horizontally and temporally averaged profiles for day three can be found in Fig. 7 for the 3.2-km analysis grid. Evident from the cloud fraction profile is a layer of cumulus near the 500-m level, which lies beneath the partly cloudy stratocumulus layer. Here most PDFs diagnose the cloud base for the underlying cumulus to be too low. The exceptions are LY, which accurately diagnoses cloud base level, and DDF, which diagnoses cloud base too high. SAM single delta function does not diagnose the cumulus layer at all. All of the more complex PDFs, as well as Single Gaussian, exhibit a slight positive bias in the cumulus layer for q_l and cloud fraction.

In the transitioning stratocumulus layer, all PDFs have a positive bias to some degree for q_l and C at the level of maximum cloud fraction, with the exception being the SAM

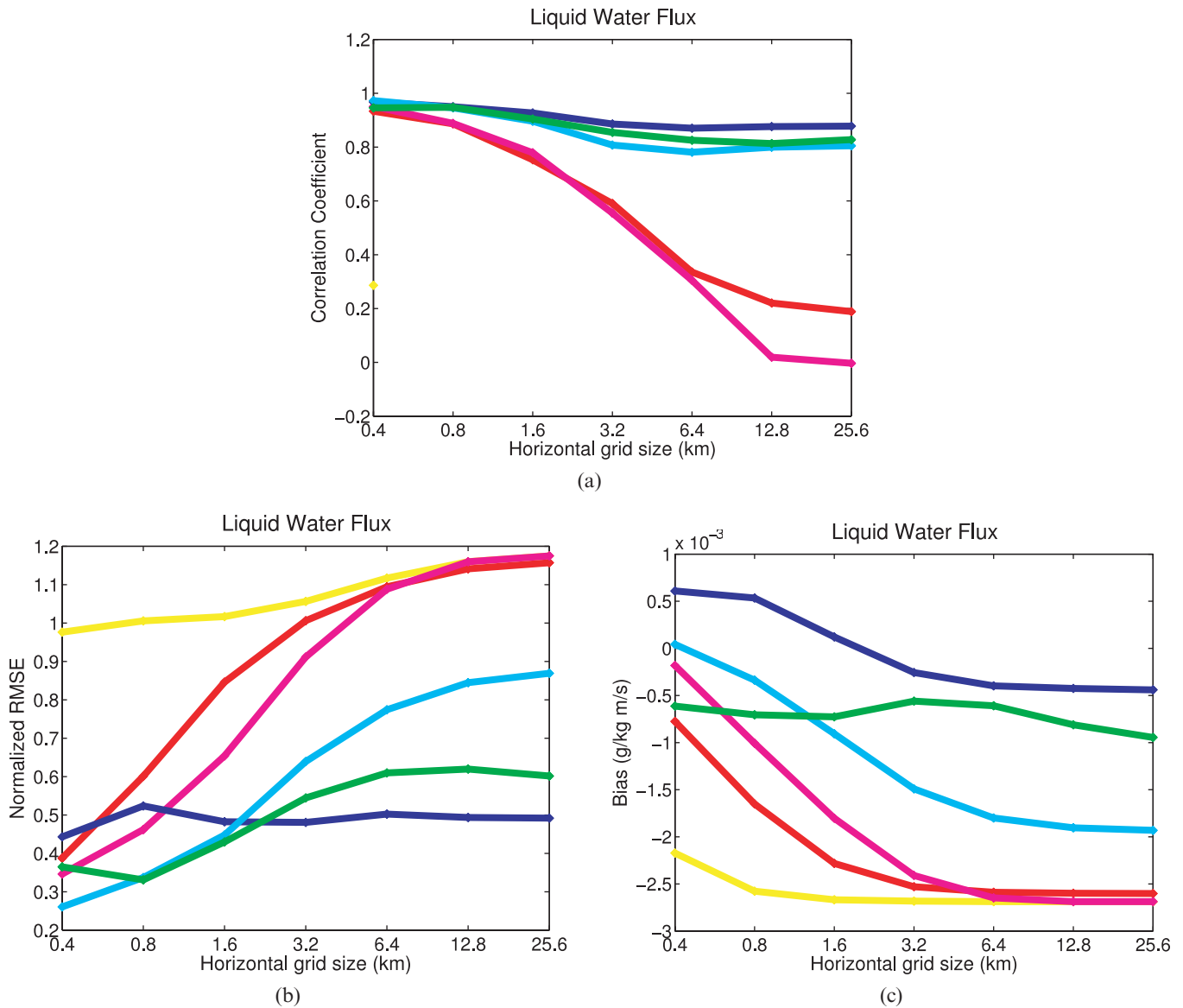


Figure 3. Statistics for liquid water flux for the BOMEX simulation for hours 3–6 for all levels. Color scheme same as Fig. 1.

single delta function. Similar analysis of the first two days (not shown), when the stratocumulus layer has a larger cloud fraction, shows accurate diagnoses by all PDFs and with no bias. By the end of the simulation, the regime has transitioned to one that resembles the BOMEX trade cumulus simulation and the PDF results are very similar to that regime.

Figure 8 shows the correlation coefficient, RMSE, and mean bias for the liquid water flux across the range of grid sizes. Similar analysis of C and q_b , while not displayed, shows that LY has a slight advantage over ADG1 & 2 PDFs. However, for $\overline{w'q'_l}$ LY clearly suffers from higher errors and lower correlation scores for most grid sizes when compared to the less complex ADG1 & 2. While ADG1 & 2 show similar skill scores in representing $\overline{w'q'_l}$, it appears that ADG1 is slightly better for the 1.6 to 3.2 km grid sizes,

while ADG2 is less biased and exhibits lower errors for the coarse grid sizes. Although these statistics are only for the third day, analysis for days one and two (when the Sc regime is present) also exhibits higher errors from the LY PDF compared to ADG1 & 2 for $\overline{w'q'_l}$.

5.3. Results from the Giga-LES of Deep Convection

5.3.1. Results of PDFs from Coarse CRM Grid Sizes

Evolution of the horizontally averaged profiles of non-precipitating cloud condensate (q_n) from the Giga-LES can be viewed in Fig. 9(a). After an hour of simulated time, the simulation is still in the spin-up process and shallow clouds are present above a very shallow mixed layer. Around hour three very light rain begins to reach the surface. After the fifth

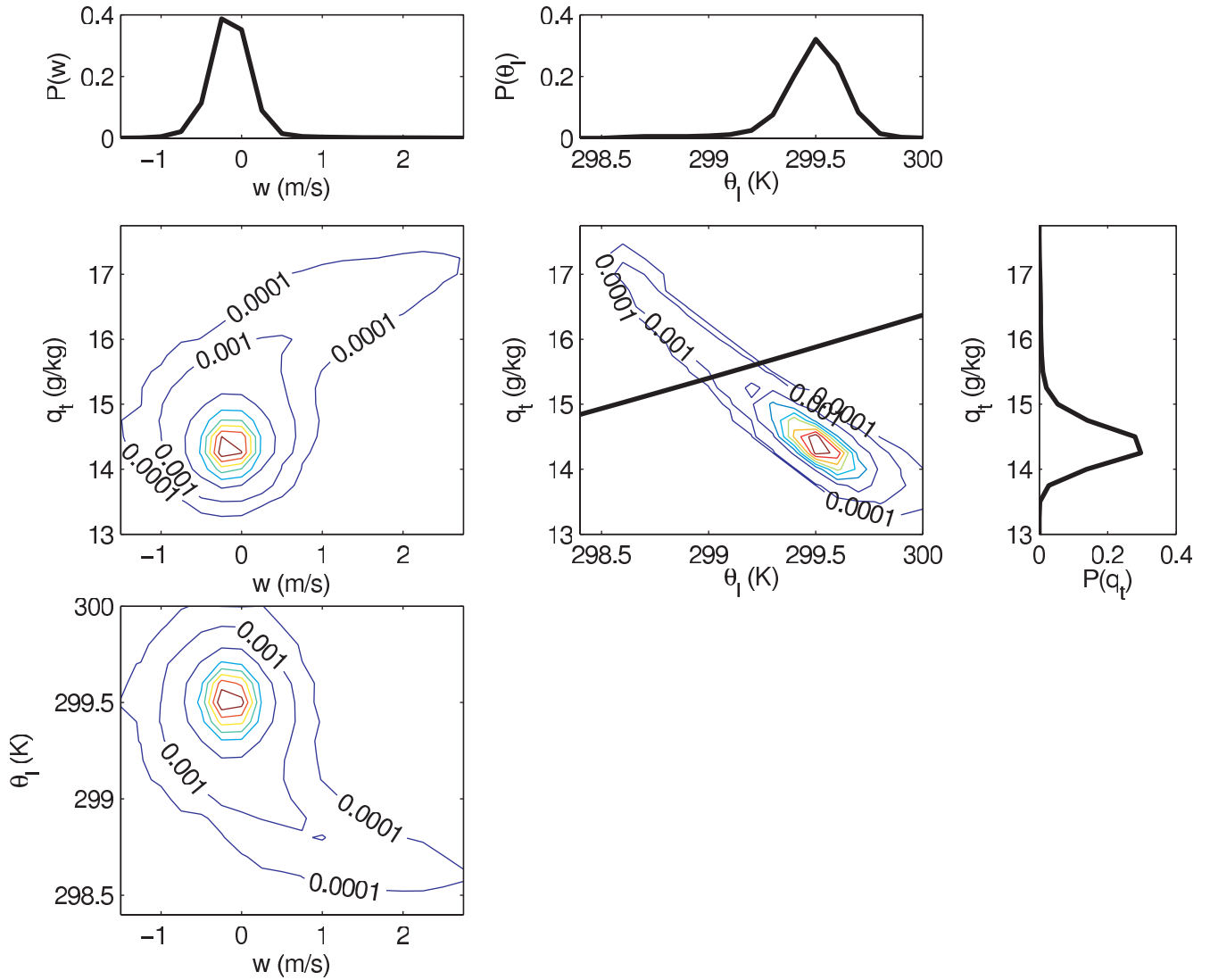


Figure 4. PDF projections computed from the 100 m benchmark BOMEX simulation in mid cloud layer (near 850 m). Black line in \bar{q}_l and θ_l projection represents the saturation curve.

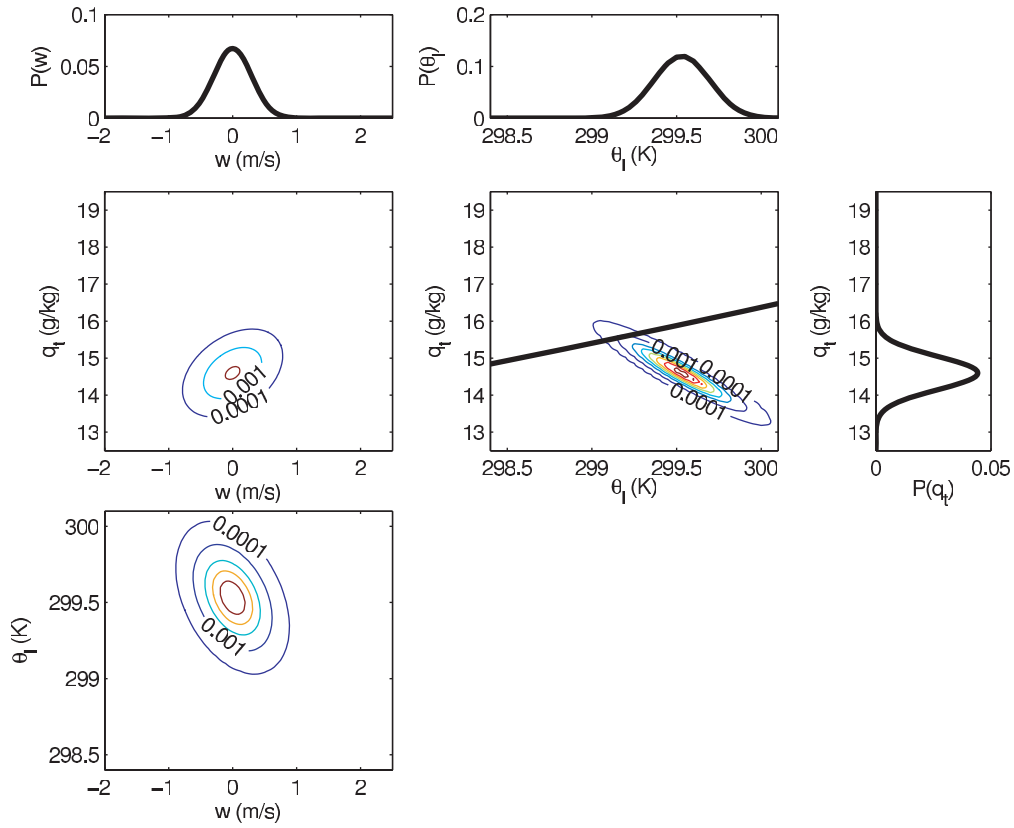
hour the shallow convection becomes more organized and is quickly followed by explosive growth of deep convection around the seventh hour, after convection reaches the freezing level (approximately 5 km). Following this event the convection and precipitation continues in a quasi-steady state.

Khairoutdinov et al. (2009) gives a complete description of the Giga-LES. However, one feature to point out from Fig. 9 is the tri-modal vertical distribution of clouds. Upper level cloud condensate maxima at hours 7, 14, and 20 are preceded by maxima of shallow cloud condensate and afterwards promote large amounts of mid-level cloudiness.

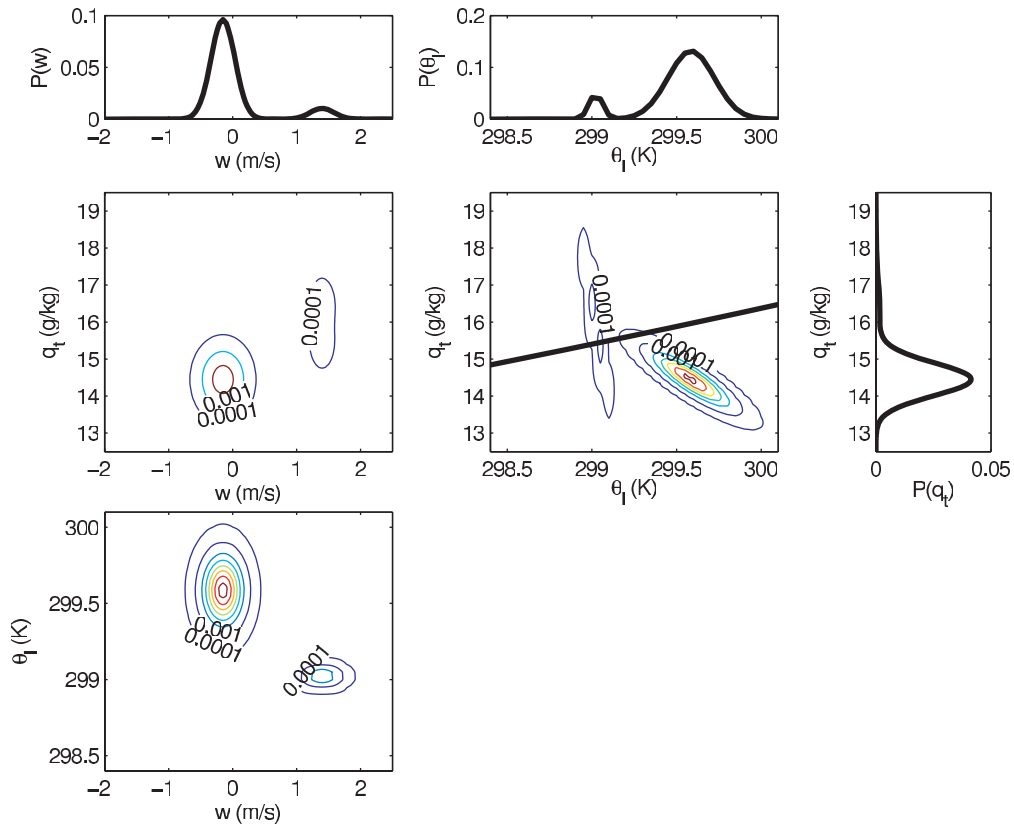
Figure 9 displays the time evolution of the horizontally averaged profiles of q_n for the 100-m grid size benchmark case, a diagnosis using the ADG1 applied at a 3.2-km analysis grid size, and a diagnosis for the SAM SDF. The averaged q_n field for the ADG1 is nicely correlated with the 100-m benchmark case. Especially important is the ability

for the ADG1 to capture the tri-modal vertical distribution of cloud condensate. However, the q_n field does have a slight positive bias for the ADG1.

The averaged q_n fields from the LY, ADG2, and SG diagnoses also resemble the ADG1 field, although they are not shown. The SAM SDF does not diagnose any low clouds (Fig. 9(c)), while the DDF diagnoses cloud base too high. In addition, DDF does not diagnose the shallow clouds that are present before the onset of deep convection. Khairoutdinov and Randall (2006) show that the precipitation and cold pools associated with these clouds are important to the formation and distribution of the deep convection. An examination of the evolution of the horizontally averaged profiles for q_n for the 6.4-km grid (not shown) shows very little differences in the vertical structure for the double gaussian based PDFs, compared to the 3.2-km analysis grid size.



(a) Single Gaussian



(b) Analytic Double Gaussian 1

Figure 5. Examples of PDF projections from trade cumulus (BOMEX case) in mid cloud layer (near 850 m) for the 25.6-km analysis grid.

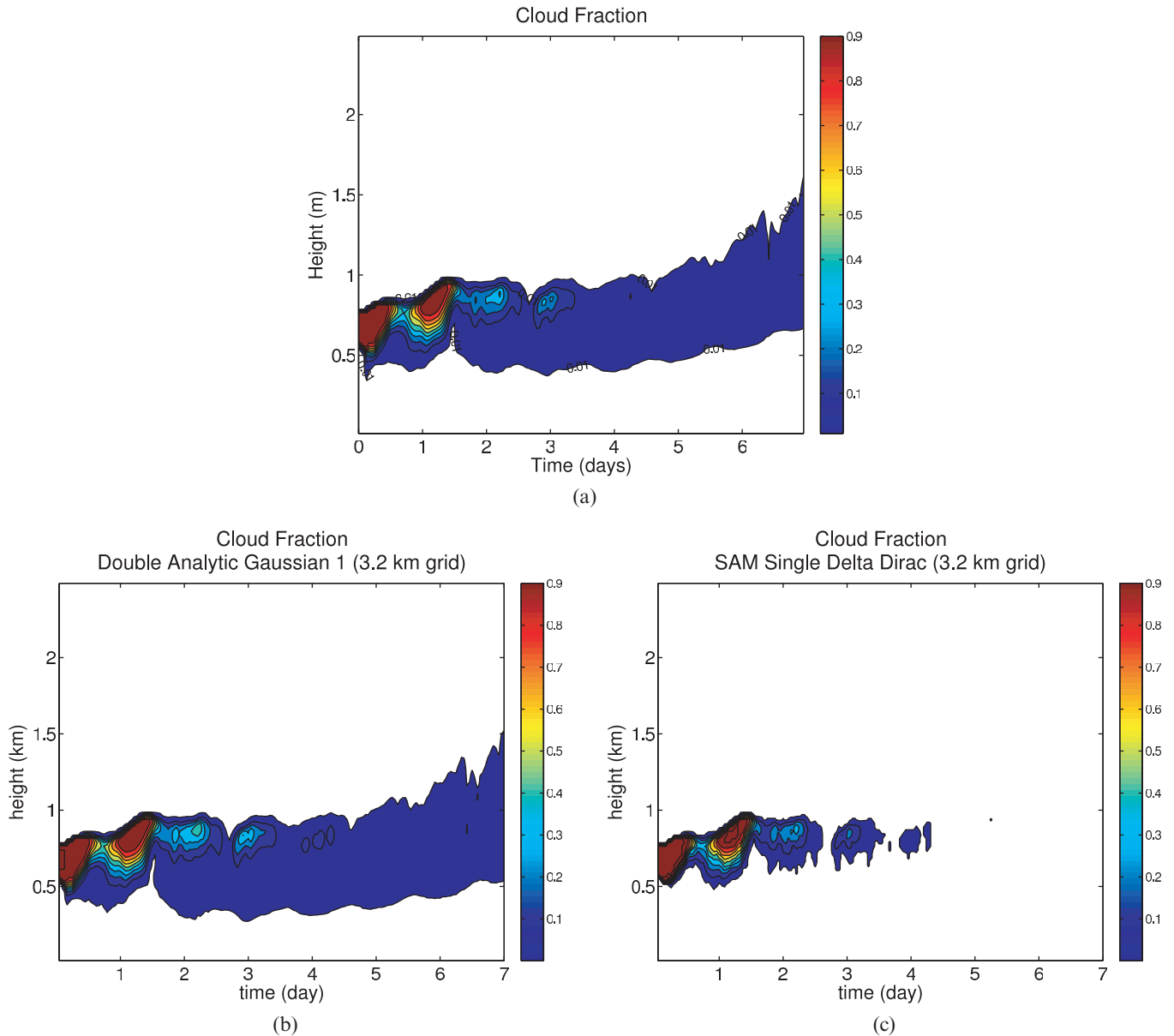


Figure 6. Time evolution of the mean profiles of non-precipitating condensed water for 100 m benchmark simulation (top) and diagnosed for a 3.2-km analysis grid (bottom) for the transition from stratocumulus to cumulus.

Horizontally and temporally averaged profiles for the 3.2 km grid of cloud fraction, q_m and SGS $w'q'_l$ for the last 12 hours of the simulation can be found in Fig. 10. Focusing first on diagnosed profiles of q_n (Fig. 10(a)), it is evident that the simpler PDFs are the outliers. Whereas SG and DDF are consistently positively biased, especially near the stratified layer at 10 km, the SAM SDF has a strong negative bias for the low clouds. The double Gaussian PDFs more realistically diagnose q_n compared to the benchmark, with ADG1 and LY matching the best.

Focusing on the lowest 5 km in Fig. 10(b) we see that for the 3.2-km grid, SG exhibits a negative bias for $w'q'_l$ as it did for BOMEX and the Sc to Cu transitions, while the SAM SDF is unable to realistically diagnose this term. Meanwhile,

the remainder of the PDFs are able to satisfactorily represent the liquid water flux for the low clouds of this complex regime.

Figure 10(c) shows the cloud fraction profiles for the last 12 hours of simulation for all levels, while Fig. 10(d) focuses on the lowest 5 km to evaluate performance for the low clouds. The cloud fraction profiles, for all PDFs, generally show good resemblance with LES profile for the upper tropospheric stratiform clouds associated with deep convection (10 km and above). Again, this result is not surprising since this layer is characterized by high cloud fraction and low skewness. However, results for the low clouds show considerable spread in the individual PDF performance. Here, all of the spatially and temporally averaged PDF

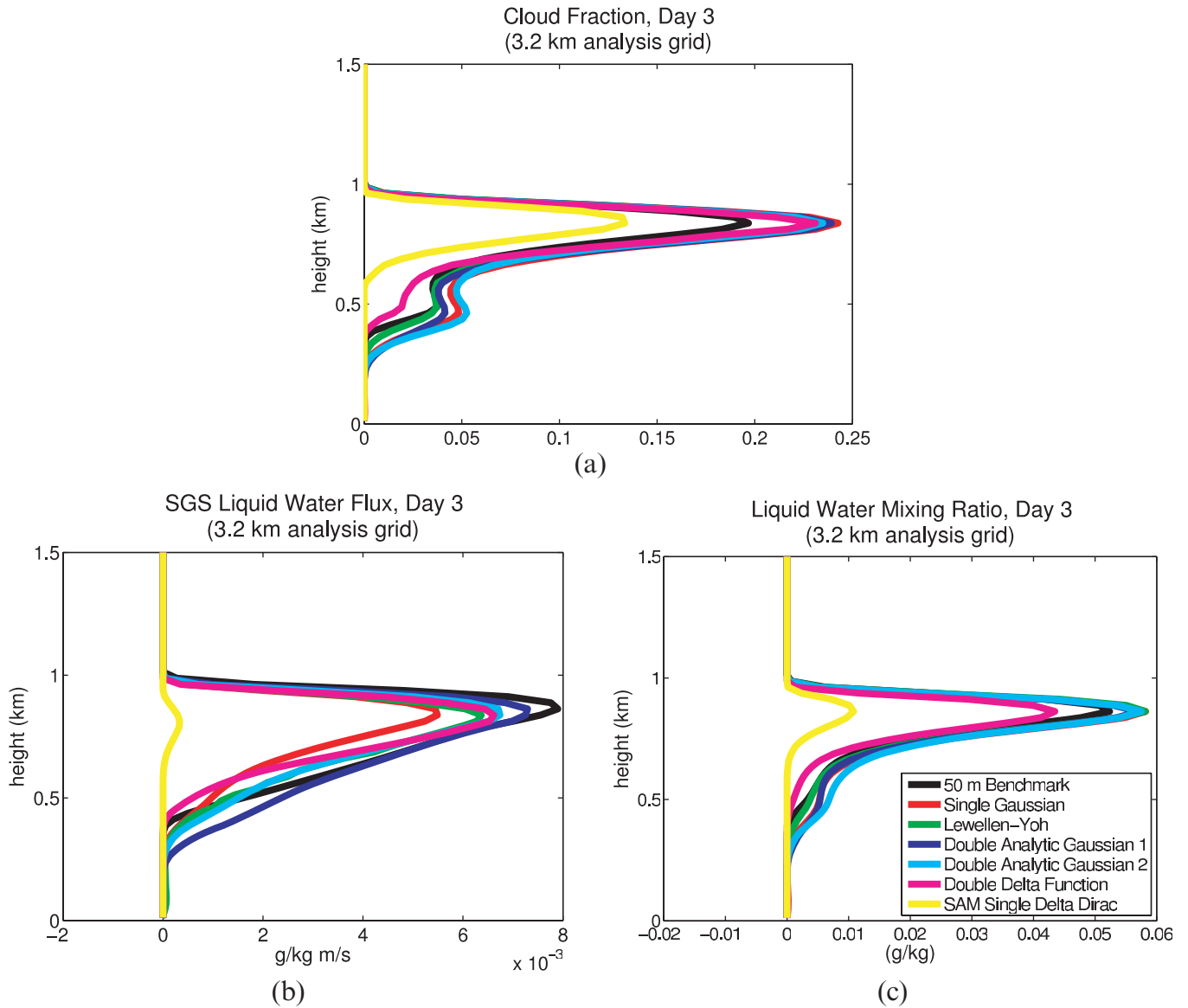


Figure 7. Same as Fig. 1, except for Profiles for day three of the Sc to Cu transition simulation.

profiles resemble the profiles of the benchmark simulation. However, most are positively biased. The exceptions are the ADG1 and LY PDFs. It has been shown (Khairoutdinov et al. 2009) that coarse-resolution simulations of the Giga-LES case produce positive biases for the low clouds that are comparable to our results of SG and ADG2. Therefore, this highlights the strengths of the ADG1 and LY PDFs, which can diagnose cloud fraction with a 3.2-km grid size with little bias. The reason for the overestimation in ADG2 is due to the fact that this PDF tends to overestimate the amplitude and width of the cloudy part of the PDF.

Figure 12 shows PDF projections for the Giga-LES for a 25.6-km grid at approximately 1 km altitude for the SG and ADG1. The selected subdomain for this case includes a deep convective core as well as shallow cumulus. The PDF computed from the benchmark simulation is shown in

Fig. 11. This regime is very different from the BOMEX case. In the Giga-LES it is possible to have contributions from several different-sized circulations: those related to shallow convection and/or those related to the mesoscale. Because the selected grid box displayed in Fig. 12 is an example of such a case, this helps to explain the overestimation seen in most of the simpler PDFs.

In this case the deep convective core is represented accurately by the ADG1 PDF (Fig. 12(b)). The deep convective core is represented by the plume with large w , low θ_b , and large q_r . However, this leaves the shallow convection and clear plumes of the grid box to be represented basically by a Single Gaussian PDF. The “shallow cumulus” portion of the PDF could lead to overrepresentation of q_l and cloud fraction and therefore is sensitive to the widths that PDF families determine and/or specify for each plume (which is

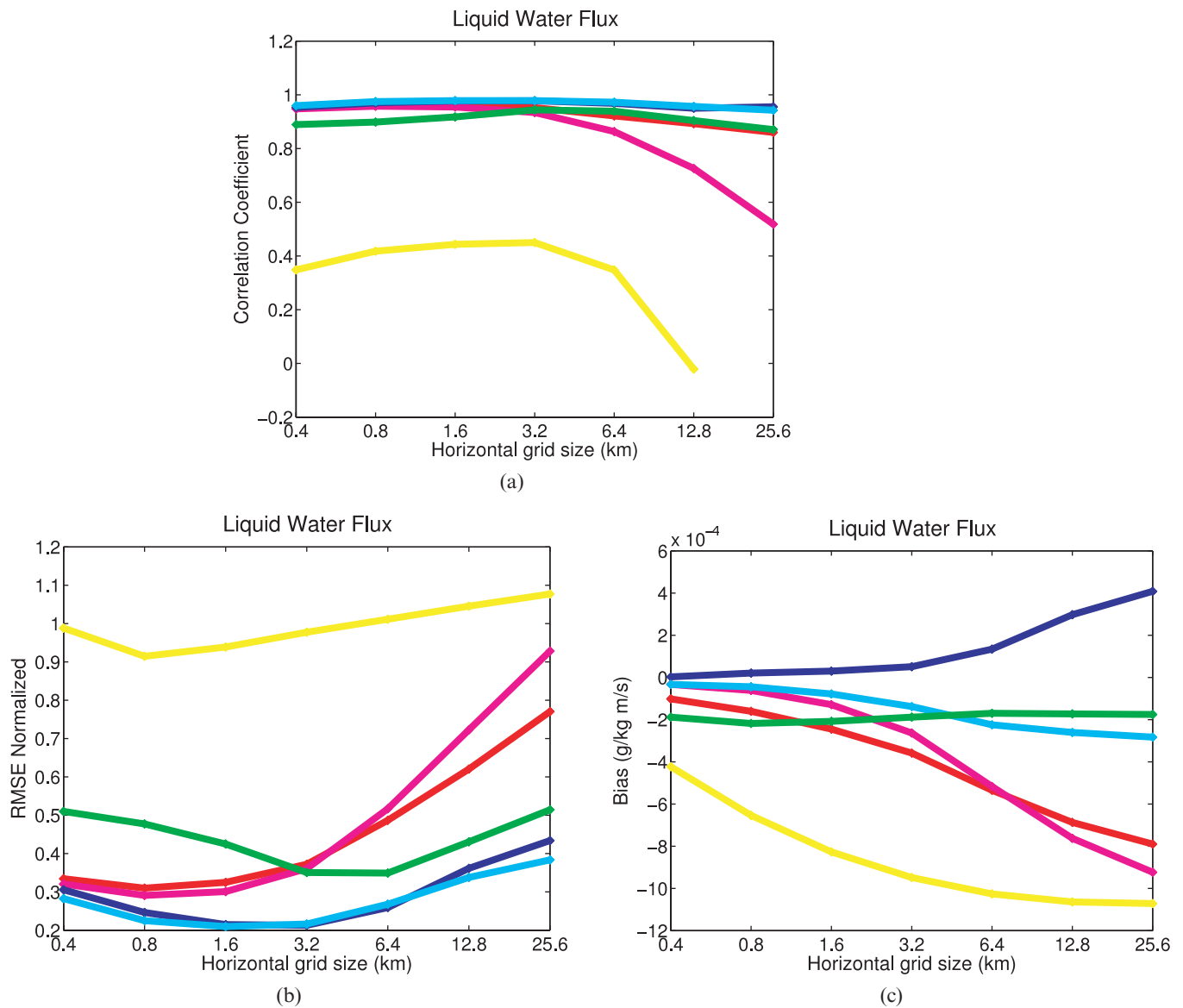


Figure 8. Statistics for liquid water flux for day three of the Sc to Cu transition simulation. Color scheme same as Fig. 1.

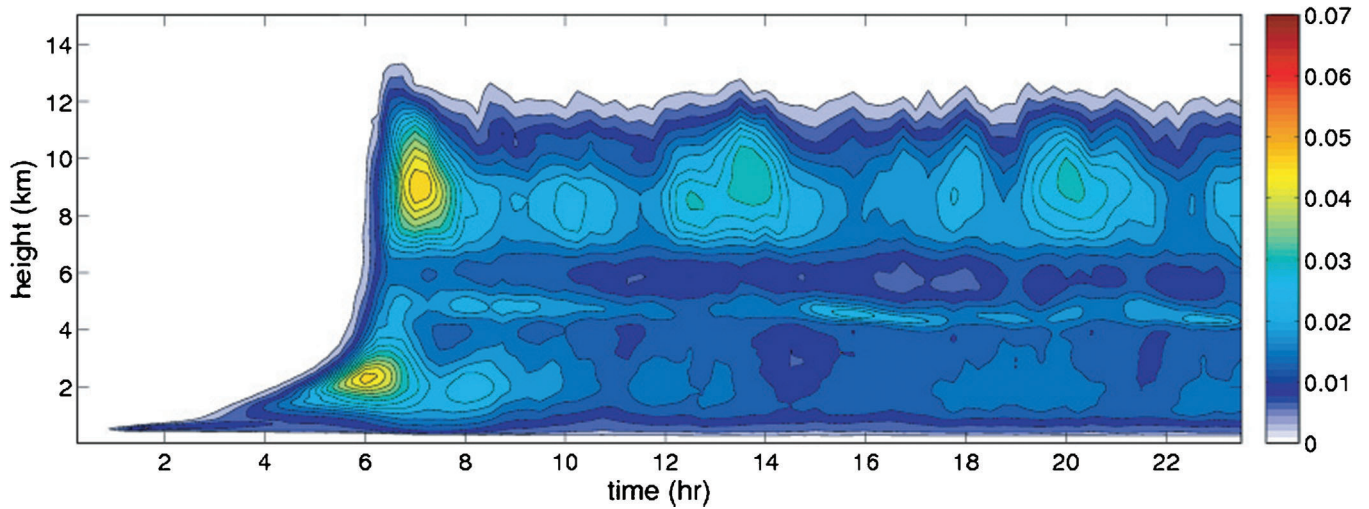
the case for ADG2). However, the case is even worse for the SG which must represent all of these plumes with just one Gaussian. For this example the benchmark LES case gives cloud fraction of 0.45, with the ADG1 diagnosing a value of 0.49 and the SG diagnosing a value of 0.72. Once again, ADG1 is able to distinguish the long tails in the distributions, where-as SG cannot. ADG2 diagnoses a cloud fraction of 0.53.

5.3.2. Horizontal Grid Size Dependence

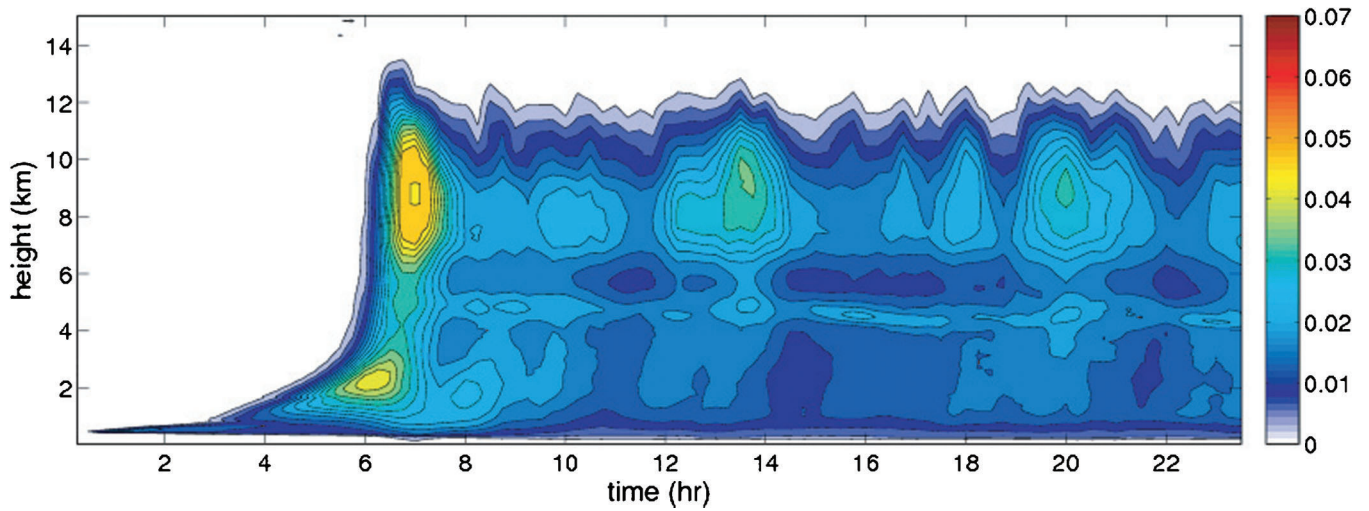
Figure 13 displays the cloud fraction statistics for each PDF family for horizontal grid sizes ranging from 0.8 km to 204.8 km (unlike the previous two cases with a minimum grid size of 0.4 km, the moments were saved during model simulation for Giga-LES and the minimum grid size was

fixed at 0.8 km). These statistics are for the lowest 5 km only, in order to emphasize the low and congestus clouds. All PDFs exhibit fairly high correlations for the small and intermediate grid sizes. The exception is the SAM SDF, for which the skill scores drops off dramatically with increasing grid size. In terms of correlation, the three double Gaussian based PDFs resemble the 100-m benchmark case more so than the less complex PDFs. However, SG and DDF provide better skill scores for the range of grid sizes compared to the other two cloud regimes, due to the fact that these PDFs are able to capture the the effects of the deep convective cores which tend to have larger cloud fractions (and hence lower skewness of the cloud properties) compared to a shallow cu regime such as BOMEX.

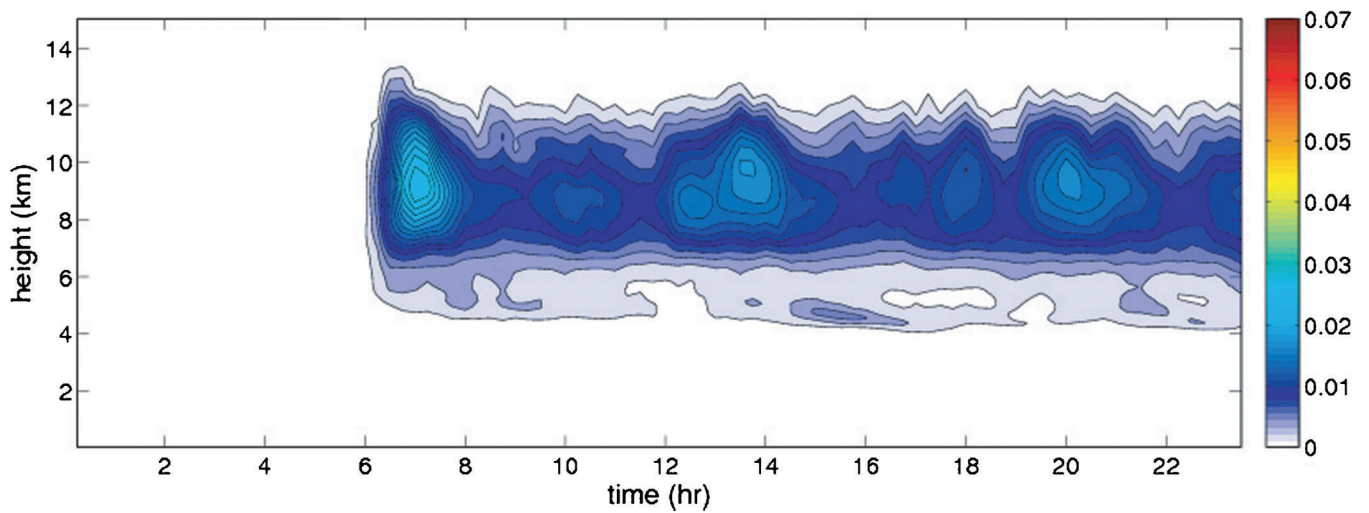
One notable feature of Fig. 13(c) is the continued trend of ADG1 to be the least biased PDF in terms of cloud fraction



(a) 100 m Benchmark



(b) 3.2 km analysis grid, Analytic. Double Gaussian 1



(c) 3.2 km analysis grid, Single Delta Function

Figure 9. Time evolution of the mean profiles of non-precipitating condensed water for 100 m benchmark simulation (top) and diagnosed for a 3.2-km analysis grid (middle and bottom) for deep convection.

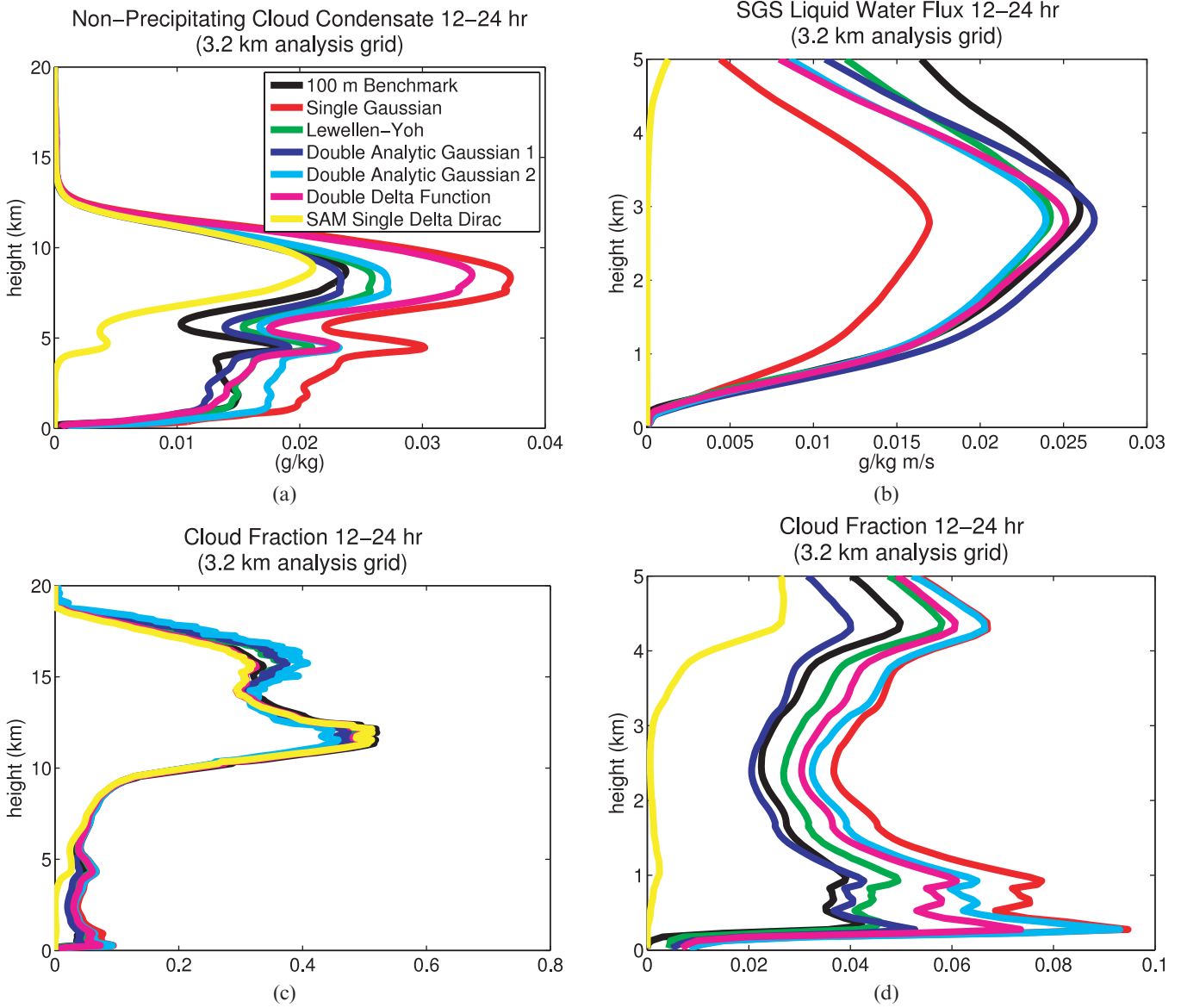


Figure 10. Same as Fig. 1, except from the last 12 hours of the Giga-LES model simulation.

(statistics for q_l are quite similar). In fact, for the larger grid sizes the ADG1 actually has a slight negative bias, which is inconsistent with the positive biases of the other PDFs. As already mentioned, it is characteristic for a coarse-grid CRM to have strong positive bias for cloud fraction of the low clouds for a deep convective regime; therefore it would not be desirable to select a PDF family that would also act to reinforce that bias. Clearly, either LY or ADG1 PDF would be the best suited families to avoid a positive bias in the low clouds.

While the three double-Gaussian-based PDFs have the lowest errors for the important intermediate grid sizes (fig. 13(b)), it is actually the DDF which exhibits the lowest errors for the largest grid sizes. Interestingly enough, the DDF also has the lowest correlation at this grid size. This can be explained by the fact that, even at the coarsest of grid

spacings, the ADG1 and ADG2 PDFs are still diagnosing good variations in the low cloud field that occur prior to and after the deep convective cycles. However, both of these PDFs are diagnosing the cloud base too low at these coarse grid sizes (not shown), leading to a higher RMSE. On the other hand, DDF does not diagnose the tri-modal vertical distribution of clouds. Overall, however, the drop in correlations for all PDFs for the 204.8 km reflects a decrease skill of diagnosing the tri-modal vertical distribution of clouds.

The correlations for $\overline{w'q_l'}$ show very interesting behavior (Fig. 14). Here we see minimum correlations for a majority of the PDFs at the 0.8 km grid spacing, with increasing scores up to the 6.4 km grid. The exceptions here are the SG and LY PDFs. A similar trend is shown in the RMSEs for which relatively high errors are exhibited by a majority of the PDFs for fine grid sizes, with LY and SG once again the

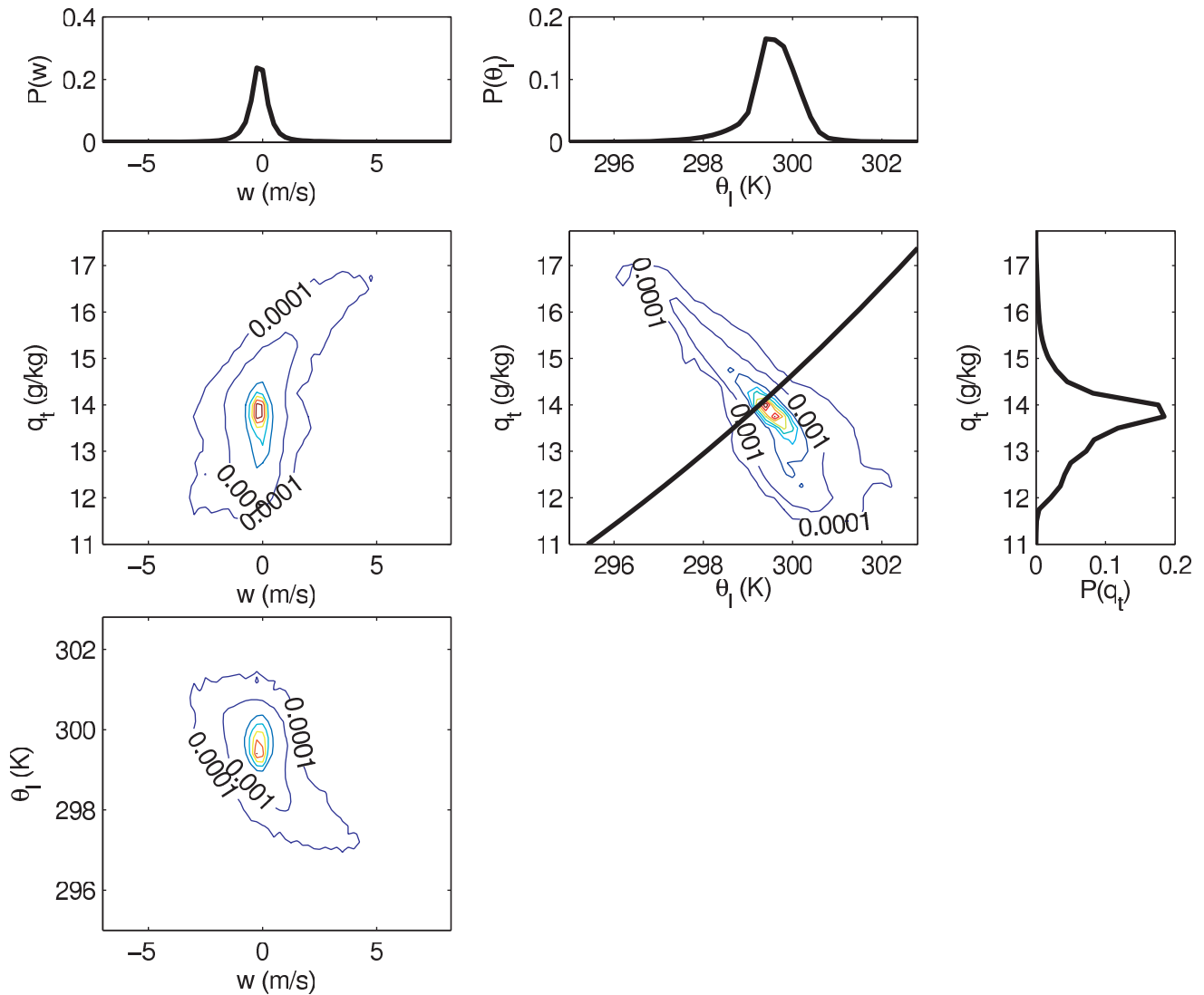


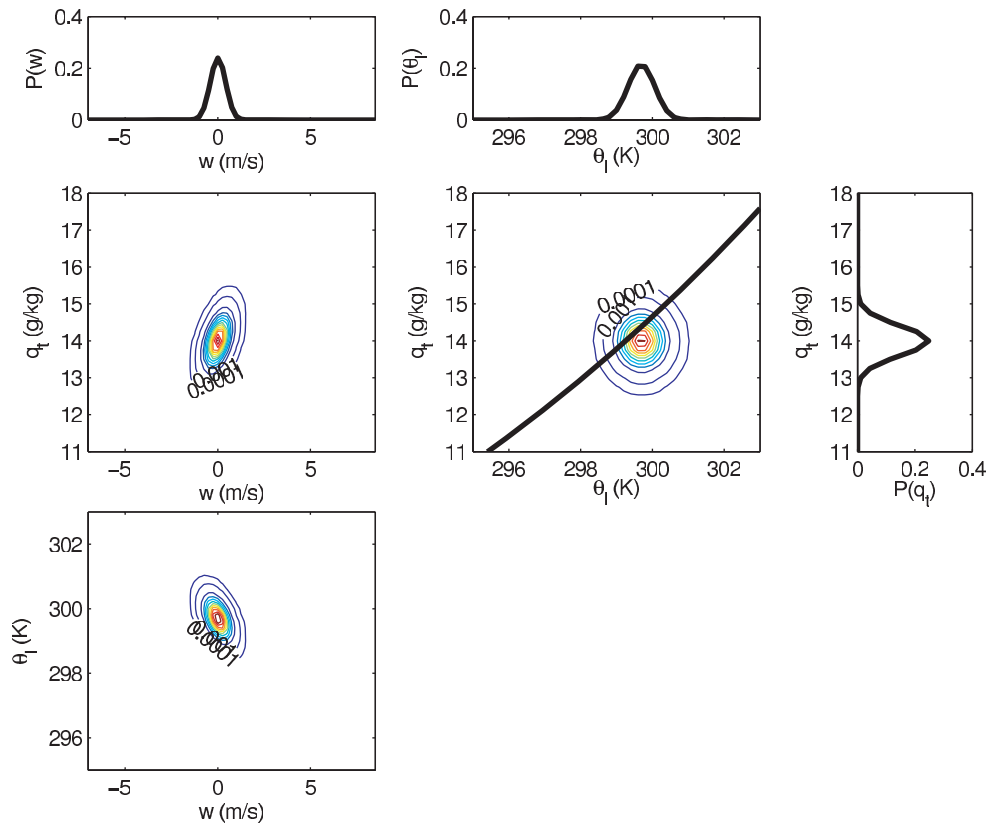
Figure 11. PDF projection from the Giga-LES for a 25.6 km x 25.6 km subdomain at 1 km.

exceptions. In general, all of the PDFs tend to best diagnose $\overline{w'q'_l}$ at the intermediate grid spacings (3.2 km to 12.8 km), which is promising for application to CRMs.

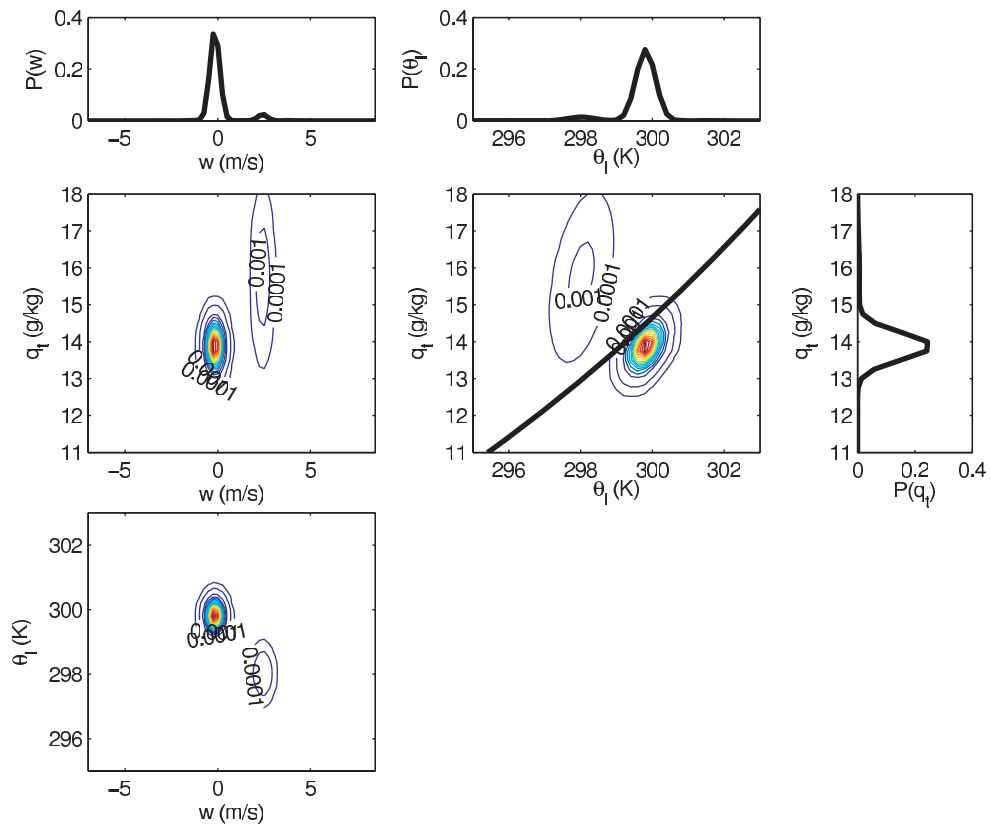
An interesting question regarding the PDF diagnosis of $\overline{w'q'_l}$ is why the LY and SG appear to represent this quantity much better than the other PDFs for fine grid spacings. It appears that at the finest grid sizes the DDF and ADG PDFs tend to diagnose the boundary layer maximum of the liquid water flux at a lower level than the 100-m benchmark case, whereas LY and SG accurately diagnose this maximum level. For the 3.2 km grid and larger sizes, all PDFs diagnose the maximum value of $\overline{w'q'_l}$ at the same height as the benchmark run. It is quite interesting, however, that a low complexity PDF and high complexity PDF are produce the same caliber results at the fine grid spacings, while the rest (mostly high complexity PDFs) do not perform quite as well.

Examination of the biases and RMSEs (Figs. 14(c) and 14(b) respectively) shows that LY, despite low errors for the

fine grid sizes, suffers from very high biases and hence errors for the coarse grid sizes. Consistent with findings from the other cases, ADG1 is the least biased PDF for the range of grid sizes, while the less complex PDFs tend to be negatively biased and the more complex PDFs positively biased. DDF and both ADG1 & 2 suffer from high RMSE for the fine grid spacings, however the mean bias scores indicate these PDFs do not have systematic bias (i.e. errors are more “randomly” distributed). In general, for the Giga-LES case, the PDF families tend to be more sensitive to grid spacing when diagnosing $\overline{w'q'_l}$, compared to the cloud fraction statistics. Most obvious is sensitivity for LY, which experiences high systematic biases for the coarse grid spacings. High errors associated with $\overline{w'q'_l}$ do not bode well for a turbulence parameterization, which relies on accurate expressions of $\overline{w'q'_l}$ for good representation of turbulence in cloudy layers. For the Giga-LES case, no family exhibits particularly consistent results across the range of grid sizes, although



(a) Single Gaussian



(b) Analytic Double Gaussian 1

Figure 12. Assumed PDF projections for a 25.6 km analysis grid at 1 km (corresponds to the subdomain in Fig. 11) for Giga-LES.

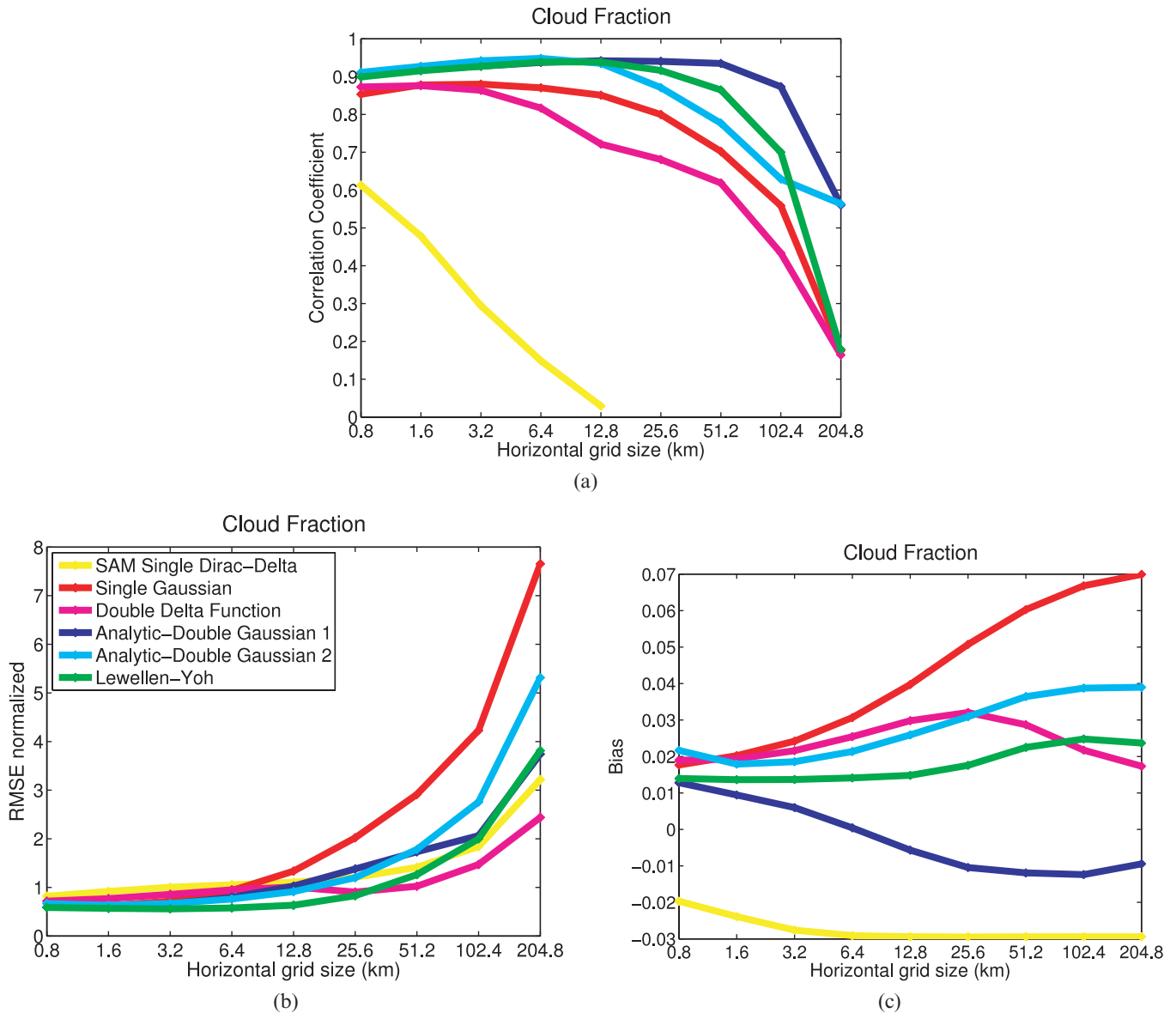


Figure 13. Statistics for cloud fraction for the Giga-LES, for the lowest 5 km and last 12 hours of model simulation.

ADG1 appears to be the best for coarse CRM size grid sizes (3.2 km or 6.4 km).

5.3.3. Sensitivity to Errors in Moments

A series of simple tests are performed to determine how sensitive the PDFs are to the introduction of errors in the input moments. The errors are introduced by simply multiplying the “perfect” second and third order moments by 0.5. Thus, the shape of the profiles for the moments remains the same and only the magnitude changes. Perhaps a more rigorous test would be to introduce random errors throughout the profile; however, the motivation behind simply changing the magnitude is that preliminary tests of diagnosing the statistical moments by the proposed parameterization generally leads to high correlation with the “perfect”

moments but contain magnitude errors (often times turbulence models underdiagnose these input moments). While future research eventually aims to reduce this problem, there are still likely to be some discrepancies and is worth while to test how the PDFs perform under such circumstances. We consider a decrease by a factor of two in the moments to hopefully be an extreme case for the errors in the diagnosed moments, and hence the worst case scenario.

These tests are performed by computing each assumed PDF with an individual moment that has been given an error (while the other input moments are kept “perfect”), to test the sensitivity to errors in individual moments. The process is repeated until each input moment has been given an error. In addition, we also perform tests with two or three input moments given errors. Finally, we perform one test in

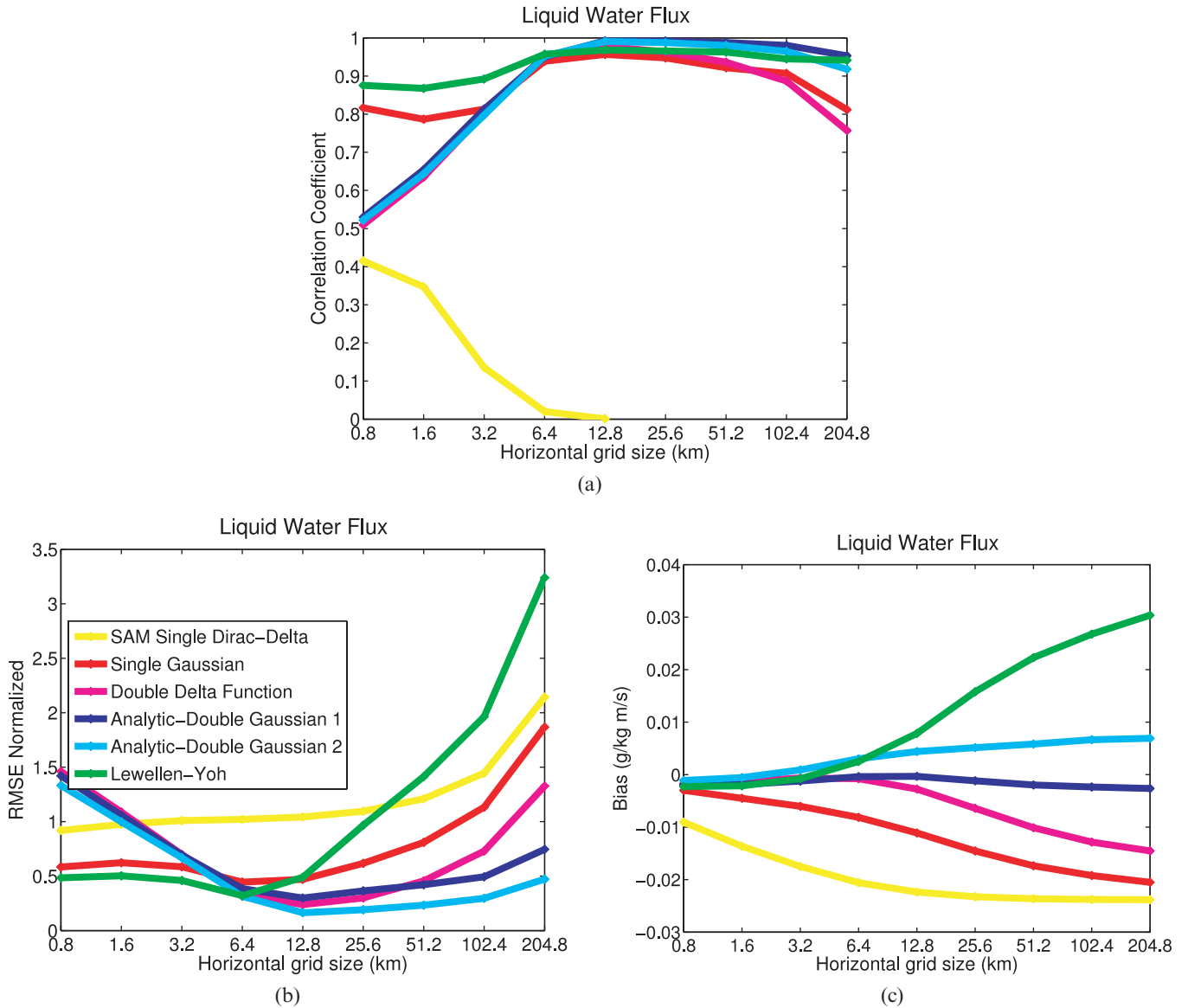


Figure 14. Statistics for liquid water flux for the Giga-LES, for the lowest 5 km and last 12 hours of model simulation.

which all second and third order moments are given errors. Here we focus discussion on the case for which all second and third order input moments are given errors, with brief discussions on the other tests that follow.

Figure 15 displays how the pattern RMSE in diagnosing $w'q'_l$ for each of the PDFs changes when errors are applied to all “perfect” second and third-order moments (Taylor 2001). Fig. 15 is for the 3.2 km analysis grid size and for the lowest 5-km of the model domain for the last 12 hours of the simulation. The benchmark simulation, or the “observation”, is displayed by the black point. As expected, the tendency is for all PDFs to lose skill when errors are introduced to the input moments. LY PDF appears to be the most sensitive PDF when errors are applied to the input moments, although it is interesting to note that the change

in correlation scores are small for all PDFs. Rather, the introduction of errors results in relatively large systematic negative biases (not represented in Fig. 15) and RMSE in $w'q'_l$. The change in RMSE is most pronounced for the LY PDF, however.

Given the fact that LY requires more input moments than both ADG PDFs, it is not surprising this PDF is more sensitive to errors. In another test, we kept the input moments of $\overline{\theta_l'^3}$ and $\overline{q_t'^3}$ “perfect” while the remaining second and third order moments were applied errors. This helps to somewhat reduce the RMSE in the LY PDF relative to when all input moments have errors. However, should LY be implemented into a CRM, it is subject to errors in both $\overline{\theta_l'^3}$ and $\overline{q_t'^3}$ which could result in higher errors associated with $w'q'_l$, relative to the other double Gaussian based PDFs.

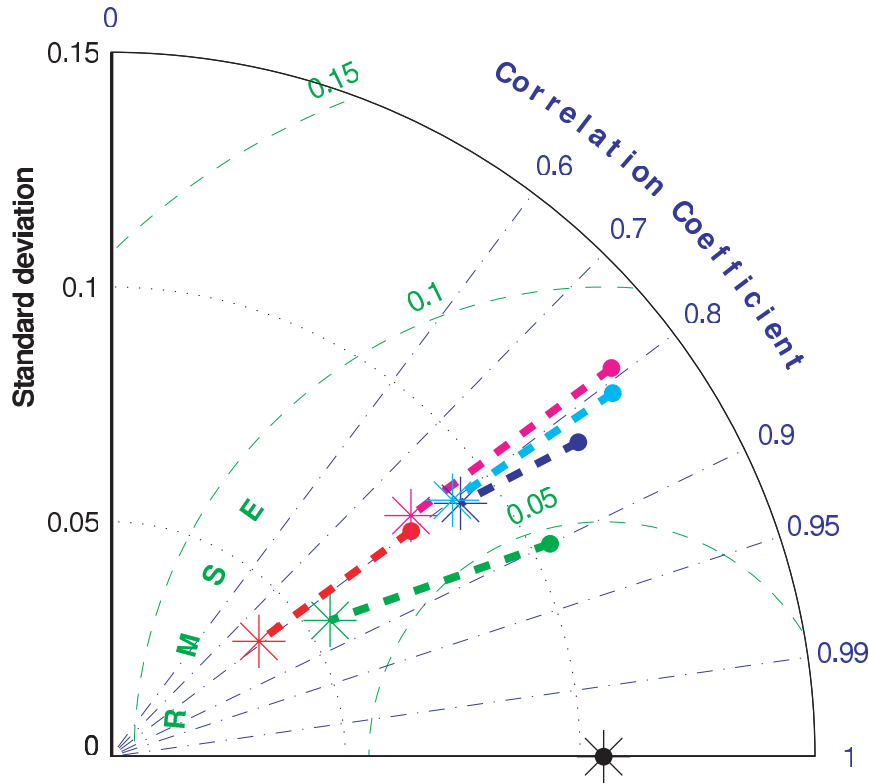


Figure 15. Taylor diagram displaying the sensitivity of the various PDFs to errors applied to the input moments for $\overline{w'q'_i}$. Star represents the statistics for each PDF after errors are applied, while the filled circle represents statistics of PDF with no errors. Black point indicates the Giga-LES 100 m benchmark. This plot is for the 3.2 km grid with errors applied to all of the second and third order input moments. Color scheme for the PDFs is the same as on the previous figure.

There are other important features from the sensitivity tests that are not illustrated. They include:

1. All PDFs appear to be most sensitive to errors applied to $\overline{w'q'_i}$ (and to a lesser degree $\overline{w'\theta'_i}$).
2. In general, C and q_n appear to be not quite as sensitive to errors in the input moments, relative to the sensitivity of $\overline{w'q'_i}$. Even with all input moments halved, all PDFs can still reasonably represent the tri-modal vertical distribution of clouds for 3.2 km and 6.4 km analysis grid sizes.
3. The tri-modal vertical distribution of clouds, however, for the coarsest grid sizes (51.2 km to 204.8 km) is completely absent for most PDFs when errors are applied. It appears that most of this contribution arises from errors in the vertical fluxes.
4. Errors applied to $\overline{w^3}$ appear to effect PDFs mostly at the coarsest grid sizes and only moderate sensitive at the fine and intermediate grid sizes. PDFs appear to be more sensitive to errors in $\overline{w^2}$ across the range of the grid box sizes.
5. A similar test is performed to that shown in Fig. 15, except with doubling the second and third order input moments. Correlation scores for C , q_n , and $\overline{w'q'_i}$ for all

PDFs are more sensitive than when input moments are halved. However, turbulence models typically underestimate these higher order moments, not overestimate. Therefore, this scenario is less likely.

The most important finding of this study is the fact that all PDFs are most sensitive to errors in $\overline{w'\theta'_i}$ and $\overline{w'q'_i}$. Therefore, a model utilizing the assumed PDF method should adequately represent these two terms. Most CRMs use eddy diffusivity (K-model) to estimate these SGS fluxes. However, Moeng et al. (2009) suggests that this downgradient diffusion model is inadequate for representing these terms for coarse grid sizes in the boundary layer and the lower portion of the cloud layer for deep convection.

5.4. Higher Order Moments

As previously mentioned, one of the advantages of the assumed PDF method is the ability to close higher order moments in an internally consistent manner. Here, evaluation of the higher order moments against those derived from the high resolution benchmark simulations are performed. We focus on validation of $\overline{w'^4}$, $\theta'_i\theta'_v$, $q'_i\theta'_v$, and $w'^2\theta'_v$ as these moments are typically needed to close model equations or are utilized in counter-gradient expressions.

The higher order moments consisting of any combination of the variables w , q_b , and θ_l can be closed by integrating over the PDF. The resulting expressions for $\overline{w^4}$, $\overline{\theta_l \theta'_v}$, $\overline{q'_l \theta'_v}$, and $\overline{w^2 \theta'_v}$ can be found in Golaz et al. (2002a). To close the buoyancy related terms mentioned, $\overline{\theta'_l q'_l}$, $\overline{q'_l q'_l}$, and $\overline{w^2 q'_l}$ must also be closed via the PDF and the expressions can be found in Larson et al. (2002). We focus our evaluation on the last six hours of the BOMEX simulation and for the 3.2 km analysis grid.

Figure 16 displays results for these higher order moments. Horizontally and temporally averaged profiles of $\overline{w^4}$ can be found in Fig. 16(a) for each PDF, as compared with the 100-m benchmark simulation. Because the Single Gaussian family is a non-skewed PDF, $\overline{w^4}$ is identically zero. DDF, on the other hand, diagnoses $\overline{w^4}$ with high correlation. However it tends to be positively biased. This is especially true in the mixed layer (approximately below 500 m) where

diagnosed magnitudes of $\overline{w^4}$ are about an order of magnitude too high. ADG1 and ADG2 are the PDFs which perform the best at diagnosing $\overline{w^4}$, with near zero bias and RMSE in the sub-cloud layer. Only in the upper cloud layer is there a slight negative bias. LY has a strong positive bias in the mixed layer but has the best representation in the cloud layer. Examination for the 6.4 km grid shows very similar results for all PDFs.

Figures 16(c) and 16(d) display the results for $\overline{q'_l \theta'_v}$ and $\overline{\theta'_l \theta'_v}$ respectively. The general behavior for the three PDFs here are similar for both of these moments. SG results are quite correlated with the terms derived from the 100 m benchmark simulation, but suffers from high biases. On the other hand, whereas ADG2 has small biases, it tends to be negatively correlated in the cloud layer for both terms. LY also suffers from some correlation issues in the cloud layer for both moments, with satisfactory representation near

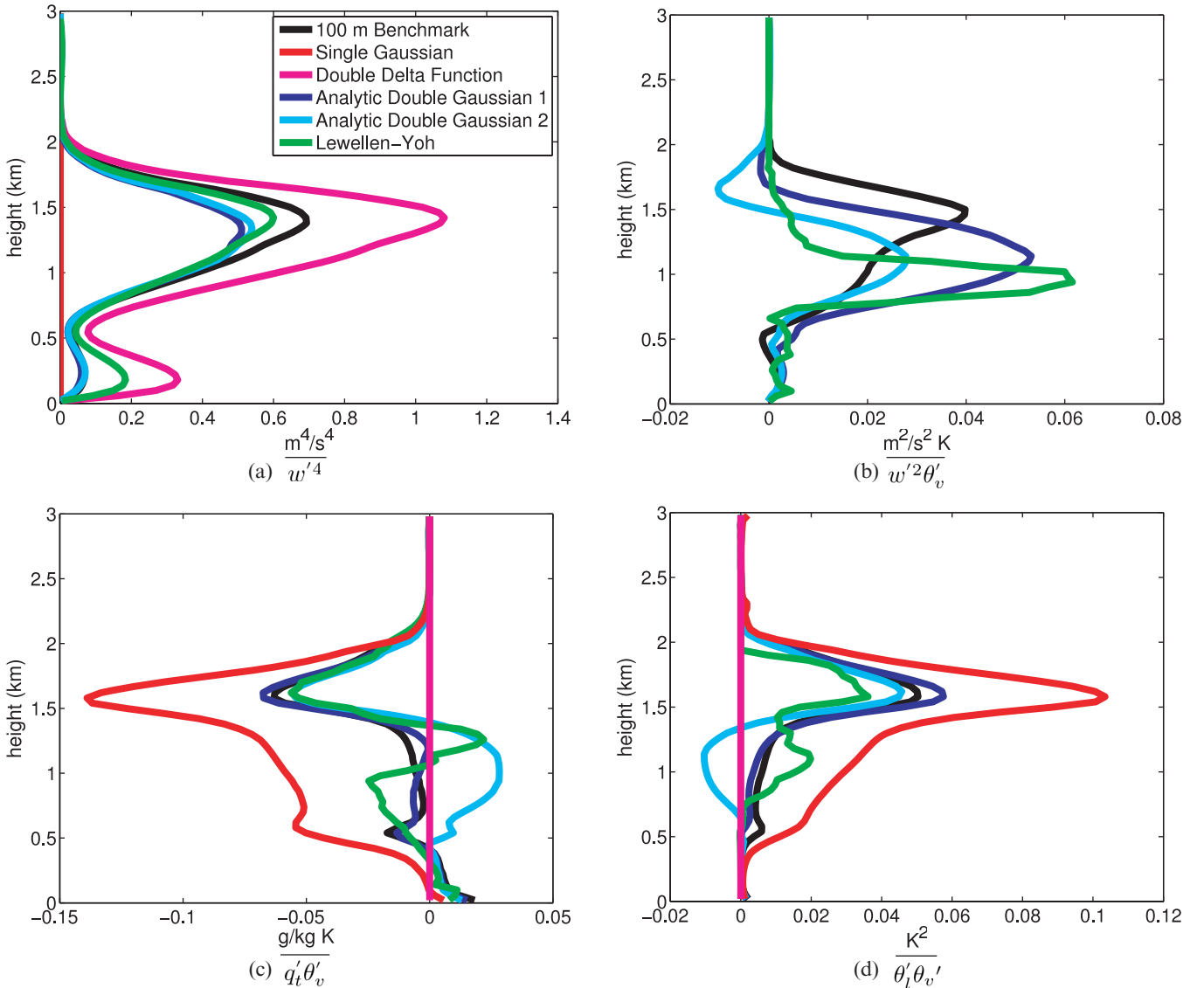


Figure 16. Profiles of higher order moments diagnosed from BOMEX simulation for the 3.2 km grid for hours 3–6.

cloud layer top. ADG1 is the only PDF family which exhibits high correlations and low biases for all levels. This further highlights the advantages of implementing this PDF family into a parameterization. These terms are zero for the DDF at every point, due to the fact that scalar variances and $\theta'_t q'_t$ do not exist for this PDF.

The last moment examined, $\overline{w^2 \theta'_v}$, is shown in Fig. 16(b). Here results for ADG1 and ADG2, while not as desirable as the previous results, still show fairly good correlation with the 100 m benchmark. The major discrepancy here is that both PDFs diagnose the maximum value of $w^2 \theta'_v$ in the middle of the cloud layer, inconsistent with the benchmark simulation where the maximum value is at the top of the cloud layer. LY diagnoses this level even lower, in the lower cloud base. However, both ADG PDFs exhibit high skill in representing this moment within the boundary layer. The SG and DDF profiles are not shown because their representations were an order of magnitude too high. It should also be noted that the skill of both ADG1 and ADG2 for diagnosing all four of these higher order moments changes little when diagnosed for the 6.4 km grid (not shown).

6. Conclusions

We extensively evaluated several PDFs to determine which are most suitable for use in coarse-grid CRMs. For this purpose, three large-eddy simulations are used as benchmarks in this study. The first simulated shallow cumulus convection based on BOMEX, the second simulated a transition from stratocumulus to cumulus, and the third, deep convection based on GATE Phase III. The latter simulation includes mesoscale organization of convection, whereas the former do not. We estimated the joint PDFs of vertical velocity (w), liquid water potential temperature (θ_l), and total water mixing ratio (q_t) using moments obtained from the benchmark simulations for horizontal grid sizes as small as 200 m to as large as 204.8 km. From each PDF, we diagnosed the cloud fraction, liquid water mixing ratio, and liquid water flux. We evaluated the performance of each PDF by comparing these quantities to the corresponding quantities obtained from the benchmark simulations.

Based on these three simulations, we found that the lower complexity PDFs (Single Delta Function, Double Delta Function, and Single Gaussian) tend to produce inconsistent results. That is, they produce fairly good results for cloud regimes that are characterized by low skewness of the cloud properties (e.g., stratocumulus) but poor results when the SGS cloud properties are more skewed (e.g., trade cumulus). Because their performance depends on SGS skewness, which increases with grid size, these PDFs are sensitive to changes in grid size, with the performance degrading as the grid size increases. For instance, the SAM SDF fails to diagnose any low clouds for intermediate (3.2 and 6.4 km) or coarse (12.8 km and higher) grid box sizes for the BOMEX and GATE cases, and fails to realistically diagnose $\overline{w'q'_l}$ for all cases. The DDF fails to adequately represent shallow

convection as it underestimates cloud fraction and q_n) but it does a satisfactory job in representing deep convective cores. SG suffers from a strong negative bias in diagnosing $\overline{w'q'_l}$ for all three simulations, even though it has a fairly good representation of q_n and cloud fraction for deep convection. Overall, the lower complexity PDFs tend to perform better for deep convection than for shallow convection for grid sizes of 12.8 km or less, due to the low skewness of SGS cloud properties in deep convection that is at least partly resolved. The lower complexity PDFs are also adequate for regimes characterized by high cloud fraction, such as stratocumulus or upper level stratiform clouds.

The three double Gaussian PDFs (Analytic Double Gaussian 1 & 2 and Lewellen-Yoh) are PDFs of higher complexity, and tend to produce more consistent results than the lower complexity PDFs. That is, they produce fairly good results for low or high skewness of the cloud properties. These PDFs exhibit high skill for most horizontal grid sizes for the three cloud regimes examined. However, ADG2 suffers from consistently high positive biases of q_m leaving LY and ADG1 as the two best performing PDFs. LY tends to slightly better represent q_n and cloud fraction, especially for shallow convection, but ADG1 has a better representation of $\overline{w'q'_l}$ (and hence the buoyancy flux). A positive bias of cloud fraction for the low clouds in the deep convective regime is characteristic of coarse-grid CRMs that employ a low complexity PDF for deep convection (Khairoutdinov et al. 2009), but both ADG1 and LY avoid this.

We also studied the sensitivity of the PDFs when errors are introduced to the input moments. Most of the PDFs are still able to reasonably represent cloud fraction, q_m and $\overline{w'q'_l}$ even under our “worst case scenario” of including errors into the input moments. However, it does appear that LY is slightly more sensitive to errors than the other double Gaussian based PDFs, likely because it requires more input moments. It is important to note that all PDFs are most sensitive to errors in the SGS vertical fluxes, $w'\theta'_l$ and $\overline{w'q'_l}$, and therefore a host model utilizing the assumed PDF method should be able to adequately parameterize these moments.

We also diagnosed various higher order moments ($\overline{w^4}$, $\theta'_l \theta'_v$, $q'_t \theta'_v$, and $\overline{w^2 \theta'_v}$). These higher-order moments are typically needed to close the equations for the second and third moments that in turn are needed to specify the double-Gaussian PDFs. ADG1 diagnoses the higher-order moments most accurately, while ADG2 and LY also produce satisfactory results.

Our general conclusions are not radically different than those of Larson et al. (2002). They showed that the more complex PDFs provided better estimates of cloud fraction, q_b and $\overline{w'q'_l}$ for the cases they examined, while SG and DDF tend to provide more unrealistic estimates. Our results confirm their findings, but over a wider range of grid sizes. The BOMEX case is the only simulation used in our study and in Larson et al. 's. Our results are generally comparable,

with differences likely arising from the more robust statistics in our study due to larger domain sizes of our simulations.

Larson et al. (2002) concluded that the Lewellen-Yoh PDF provided the best matches to aircraft data and LES results. Had our study of PDF performance only included shallow boundary layer clouds (e.g. BOMEX and the transition case), as Larson et al. (2002) did, then we would likely arrive at the same conclusion. However, we found that ADG1 is less sensitive than LY to input moment errors, and that ADG1 exhibits better skill in diagnosing higher order moments. Also of concern are the sometimes higher errors for LY in diagnosing $\overline{w'q'_l}$, such as those seen in coarse grid box sizes for deep convection and, to a lesser degree, in the transition case (however, it should be noted that LY does have the best representation of $\overline{w'q'_l}$ for the fine grid sizes for deep convection). This result is not unique to our study, as Larson et al. (2002) also found high errors for $\overline{w'q'_l}$ diagnosed from the LY family in their stratocumulus case (Fig. 7 of their paper). As already stated, the importance of accurate representation of $\overline{w'q'_l}$ within cumulus layers is crucial for any turbulence parameterization.

Although LY may provide somewhat better fits for shallow convection cloud properties (such as the locations of cloud top and cloud base), there appears to be little difference in skill for deep convection when compared to ADG1. In addition, ADG1 appears to be better at diagnosing $\overline{w'q'_l}$ for most cases and grid sizes examined. ADG1 is also a less complex PDF than LY because it does not require θ_l^3 or q_l^3 as inputs, nor does it require a numerical root finder. Golaz et al. (2002a) took this into consideration when selecting ADG1 for their single column model. Therefore, we conclude that while both LY and ADG1 have their strengths and weaknesses, it does not appear that either one is decisively better than the other. However, due to the reduced computational cost associated with ADG1, relative to LY, it appears that this PDF family is ideal for implementation into a coarse-grid CRM that is embedded into a MMF.

Future work will involve utilizing the ADG1 PDF in a SGS turbulence closure for coarse-grid CRMs and testing the closure in CRM simulations. While the addition of the assumed PDF aims to improve SGS turbulence and cloud representation in coarse-grid CRMs, it does not address other SGS problems in CRMs and GCMs. These include representing the SGS variability in microphysical process rates and radiative fluxes, for example. However, representing these may not as critical in a coarse-grid CRM (which resolves the mesoscale as well as some of the deep convective variability) as in a GCM.

Acknowledgments: This material is based upon work supported by the National Science Foundation Science and Technology Center for Multi-Scale Modeling of Atmospheric Processes, managed by Colorado State University under cooperative agreement No. ATM-0425247. We would like to acknowledge high performance computing support

provided by NCAR's Computational and Information Systems Laboratory, sponsored by the National Science Foundation. The Giga-LES was performed using the IBM BlueGene/L "New York Blue supercomputer at the New York Center for Computational Sciences, which is a joint venture of Stony Brook University and Brookhaven National Laboratory. The authors would also like to thank two anonymous reviewers for very useful comments.

References

- Arakawa, A., 2004: The cumulus parameterization problem: Past, present, and future. *J. Climate*, **13**, 2493–2525, doi: [10.1175/1520-0442\(2004\)017<2493:RATCPP>2.0.CO;2](https://doi.org/10.1175/1520-0442(2004)017<2493:RATCPP>2.0.CO;2).
- Arakawa, A., and W. H. Schubert, 1974: Interaction of a cumulus cloud ensemble with the large-scale environment, Part I. *J. Atmos. Sci.*, **31**, 674–701, doi: [10.1175/1520-0469\(1974\)031<0674:IOACCE>2.0.CO;2](https://doi.org/10.1175/1520-0469(1974)031<0674:IOACCE>2.0.CO;2).
- Bechtold, P., C. Fravallo, and J. P. Pinty, 1992: A model of marine boundary-layer cloudiness for mesoscale applications. *J. Atmos. Sci.*, **49**, 10.1175/1723–1744, doi: [10.1175/1520-0469\(1992\)049<1723:AMOMBL>2.0.CO;2](https://doi.org/10.1175/1520-0469(1992)049<1723:AMOMBL>2.0.CO;2).
- Bougeault, P., 1981a: Modeling the trade-wind cumulus boundary layer. Part I: Testing the ensemble cloud relations against numerical data. *J. Atmos. Sci.*, **38**, 2414–2428, doi: [10.1175/1520-0469\(1981\)038<2414:MTTWCB>2.0.CO;2](https://doi.org/10.1175/1520-0469(1981)038<2414:MTTWCB>2.0.CO;2).
- Bougeault, P., 1981b: Modeling the trade-wind cumulus boundary layer. Part II: A higher-order one-dimensional model. *J. Atmos. Sci.*, **38**, 2429–2439, doi: [10.1175/1520-0469\(1981\)038<2429:MTTWCB>2.0.CO;2](https://doi.org/10.1175/1520-0469(1981)038<2429:MTTWCB>2.0.CO;2).
- Bretherton, C. S., 1993: Understanding Albrecht's model of trade cumulus cloud fields. *J. Atmos. Sci.*, **50**, 2264–2283, doi: [10.1175/1520-0469\(1993\)050<2264:UAMOTC>2.0.CO;2](https://doi.org/10.1175/1520-0469(1993)050<2264:UAMOTC>2.0.CO;2).
- Golaz, J. C., V. E. Larson, and W. R. Cotton, 2002a: A pdf-based model for boundary layer clouds part I: Method and model description. *J. Atmos. Sci.*, **59**, 3540–3551, doi: [10.1175/1520-0469\(2002\)059<3540:APBMFB>2.0.CO;2](https://doi.org/10.1175/1520-0469(2002)059<3540:APBMFB>2.0.CO;2).
- Golaz, J. C., V. E. Larson, and W. R. Cotton, 2002b: A pdf-based model for boundary layer clouds part II: Model results. *J. Atmos. Sci.*, **59**, 3552–3571, doi: [10.1175/1520-0469\(2002\)059<3552:APBMFB>2.0.CO;2](https://doi.org/10.1175/1520-0469(2002)059<3552:APBMFB>2.0.CO;2).
- Grabowski, W. and P. Smolarkiewicz, 1999: CRCP: A cloud resolving convection parameterization for modeling the tropical convective atmosphere. *Physic. D.*, **133**, 171–178, doi: [10.1016/S0167-2789\(99\)00104-9](https://doi.org/10.1016/S0167-2789(99)00104-9).
- Holland, J. and E. Rasmusson, 1973: Measurement of atmospheric mass, energy and momentum budgets over a 500-kilometer square of tropical ocean. *Mon. Wea. Rev.*, **101**, 44–55, doi: [10.1175/1520-0493\(1973\)101<0044:MOTAME>2.3.CO;2](https://doi.org/10.1175/1520-0493(1973)101<0044:MOTAME>2.3.CO;2).
- Khairoutdinov, M. F. and D. A. Randall, 2003: Cloud resolving modeling of the ARM summer 1997 IOP: Model formulations, results, uncertainties, and sensitiv-

- ities. *J. Atmos. Sci.*, **60**, 607–625, doi: [10.1175/1520-0469\(2003\)060<0607:CRMOTA>2.0.CO;2](https://doi.org/10.1175/1520-0469(2003)060<0607:CRMOTA>2.0.CO;2).
- Khairoutdinov, M. F. and D. A. Randall, 2006: High-resolution simulation of shallow-to-deep convection transition over land. *J. Atmos. Sci.*, **63**, 3421–3436, doi: [10.1175/JAS3810.1](https://doi.org/10.1175/JAS3810.1).
- Khairoutdinov, M. F., D. A. Randall, and C. Dermott, 2005: Simulations of the atmospheric general circulation using a cloud-resolving model as a superparameterization of physical processes. *J. Atmos. Sci.*, **62**, 2136–2154, doi: [10.1175/JAS3453.1](https://doi.org/10.1175/JAS3453.1).
- Khairoutdinov, M. F., S. K. Krueger, C.-H. Moeng, P. Bogenschutz, and D. A. Randall, 2009: Large-eddy simulation of maritime deep tropical convection. *J. Adv. Model. Earth Syst.*, **Vol. 1**, Art. # 15, 13 pp., doi: [10.3894/JAMES.2009.1.15](https://doi.org/10.3894/JAMES.2009.1.15).
- Klein, S. A., D. L. Hartmann, and J. R. Norris, 1995: On the relationships among low clouds structure, sea surface temperature, and atmospheric circulation in the summertime northeast Pacific. *J. Climate*, **8**, 1140–1155, doi: [10.1175/1520-0442\(1995\)008<1140:OTRALC>2.0.CO;2](https://doi.org/10.1175/1520-0442(1995)008<1140:OTRALC>2.0.CO;2).
- Krueger, S. K., 1988: Numerical simulation of tropical cumulus clouds and their interaction with the subcloud layer. *J. Atmos. Sci.*, **45**, 2221–2250, doi: [10.1175/1520-0469\(1988\)045<2221:NSOTCC>2.0.CO;2](https://doi.org/10.1175/1520-0469(1988)045<2221:NSOTCC>2.0.CO;2).
- Krueger, S. K., G. McLean, and Q. Fu, 1995: Numerical simulation of the stratus-to-cumulus transition in the subtropical boundary layer. Part I: Boundary-layer structure. *J. Atmos. Sci.*, **52**, 2839–2850, doi: [10.1175/1520-0469\(1995\)052<2839:NSOTST>2.0.CO;2](https://doi.org/10.1175/1520-0469(1995)052<2839:NSOTST>2.0.CO;2).
- Lappen, C. and D. A. Randall, 2001: Toward a unified parameterization of the boundary layer and moist convection. Part I: A new type of mass flux model. *J. Atmos. Sci.*, **58**, 2021–2036, doi: [10.1175/1520-0469\(2001\)058<2021:TAUPOT>2.0.CO;2](https://doi.org/10.1175/1520-0469(2001)058<2021:TAUPOT>2.0.CO;2).
- Larson, V. E., J. C. Golaz, and W. R. Cotton, 2002: Smallscale and mesoscale variability in cloud boundary layers: Joint probability density functions. *J. Atmos. Sci.*, **59**, 3519–3539, doi: [10.1175/1520-0469\(2002\)059<3519:SSAMVI>2.0.CO;2](https://doi.org/10.1175/1520-0469(2002)059<3519:SSAMVI>2.0.CO;2).
- Lewellen, W. S. and S. Yoh, 1993: Binormal model of ensemble partial cloudiness. *J. Atmos. Sci.*, **50**, 1228–1237, doi: [10.1175/1520-0469\(1993\)050<1228:BMOEPC>2.0.CO;2](https://doi.org/10.1175/1520-0469(1993)050<1228:BMOEPC>2.0.CO;2).
- Luhar, A., M. Hibberd, and P. Hurley, 1996: Comparison of closure schemes used to specify the velocity PDF in langrangian stochastic dispersion models for convective conditions. *Atmos. Environ.*, **30**, 1407–1418, doi: [10.1016/1352-2310\(95\)00464-5](https://doi.org/10.1016/1352-2310(95)00464-5).
- Moeng, C.-H., M. A. LeMone, M. F. Khairoutdinov, S. K., Krueger, P. Bogenschutz, and D. A. Randall, 2009: The tropical marine boundary layer under a deep convection system: a large-eddy simulation study. *J. Adv. Model. Earth Syst.*, **Vol. 1**, Art. #16, 13 pp., doi: [10.3894/JAMES.2009.1.16](https://doi.org/10.3894/JAMES.2009.1.16).
- Randall, D. A., 1980: Conditional instability of the first kind, upside-down. *J. Atmos. Sci.*, **37**, 125–130. doi: [10.1175/1520-0469\(1980\)037<0125:CIOTFK>2.0.CO;2](https://doi.org/10.1175/1520-0469(1980)037<0125:CIOTFK>2.0.CO;2).
- Randall, D. A., M. Khairoutdinov, A. Arakawa, and W. Grabowski, 2003: Breaking the cloud-parameterization deadlock. *J. Atmos. Sci.*, **60**, 1547–1564, doi: [10.1175/BAMS-84-11-1547](https://doi.org/10.1175/BAMS-84-11-1547).
- Redelsperger, J. L. and G. Sommeria, 1986: Three-dimensional simulation of a convective storm: Sensitivity studies on subgrid parameterization and spatial resolution. *J. Atmos. Sci.*, **43**, 2619–2635, doi: [10.1175/1520-0469\(1986\)043<2619:TDSOAC>2.0.CO;2](https://doi.org/10.1175/1520-0469(1986)043<2619:TDSOAC>2.0.CO;2).
- Siebesma, A. Pier, C. S. Bretherton, A. Brown, A. Chlond, J. Cuxart, P. G. Duynkerke, H. Jiang, M. Khairoutdinov, D. Lewellen, C.-H. Moeng, E. Sanchez, B. Stevens and D. EStevens, 2003: A large eddy simulation intercomparison study of shallow cumulus convection. *J. Atmos. Sci.*, **60**, 1201–1219, doi: [10.1175/1520-0469\(2003\)60<1201:ALESIS>2.0.CO;2](https://doi.org/10.1175/1520-0469(2003)60<1201:ALESIS>2.0.CO;2).
- Slingo, A., 1990: Sensitivity of the Earth's radiation budget to changes in low clouds. *Nature*, **343**, 49–51, doi: [10.1038/343049a0](https://doi.org/10.1038/343049a0).
- Taylor, Karl E., 2001: Summarizing multiple aspects of model performance in a single diagram, *J. Geophys. Res.*, **106**, 7183–7192, doi: [10.1029/2000JD900719](https://doi.org/10.1029/2000JD900719).
- Tiedtke, M., 1988: Parameterization of cumulus convection in large-scale models. *Physically-Based Modeling and Simulation of Climate and Climate Change*, Schlesinger, Ed., D. Reidel, 375–431.